Dual carbon isotope-based source apportionment and light absorption properties of water soluble organic carbon in PM 2.5 over China

Yangzhi Mo[1], Jun Li[2], Zhineng Cheng[2], Guangcai Zhong[2], Sanyuan Zhu[2], Chongguo Tian[3], Yingjun Chen[4], and Gan Zhang[2]

[1]Guangzhou Institute of Geochemistry, Chinese Academy of Sciences
[2]Guangzhou Institute of Geochemistry
[3]Yantai Institute of Coastal Zone Research, Chinese Academy of Science
[4]Fudan University

November 28, 2022

Abstract

Water soluble organic carbon (WSOC) makes up a large fraction of organic carbon, which attracted great attention due to its light absorption properties and human health effects. Sources and light absorption properties of WSOC in 10 cities across China were studied by dual carbon isotope analysis and UV-visible spectrophotometer, respectively. Despite the dominate contribution of non-fossil sources, the fossil sources contribution of WSOC in China was higher than other regions across the world. The average MAE365 and fossil sources contribution of WSOC was 1.13 ± 0.37 m2/gC and 39.9 ± 9.4%, both of which were higher in Northern China. The non-fossil sources contribution of WSOC and MAE365, WSOC exhibited significant seasonal variations with highest values during cold seasons, which was likely associated with corn residues burning. Compared to warm seasons, the MAE365, WSOC showed a positive relationship with relative contribution of fossil sources and with higher values during cold seasons, indicating the fossil derived WSOC had higher light absorption capacity and enhance the overall color of WSOC during cold seasons. To constraining the regional climate and health impact of WSOC, this study suggests that mitigation strategy should consider the spatiotemporal variations in the sources, formation pathways and light absorption properties of WSOC.

Hosted file

essoar.10505115.1.docx available at https://authorea.com/users/557095/articles/606843-dual-carbon-isotope-based-source-apportionment-and-light-absorption-properties-of-water-soluble-organic-carbon-in-pm-2-5-over-china

Dual carbon isotope-based source apportionment and light absorption properties of water soluble organic carbon in $PM_{2.5}$ over China

Yangzhi Mo[1], Jun Li[1*], Zhineng Cheng[1], Guangcai Zhong[1], Sanyuan Zhu[1], Chongguo Tian[2], Yingjun Chen[3], Gan Zhang[1*]

[1] State Key Laboratory of Organic Geochemistry and Guangdong Key Laboratory of Environmental Protection and Resources Utilization, Guangzhou Institute of Geochemistry, Chinese Academy of Sciences, Guangzhou 510640, China

[2] Key Laboratory of Coastal Zone Environmental Processes and Ecological Remediation, Yantai Institute of Coastal Zone Research, Chinese Academy of Science, Yantai, 264003, China

[3]Shanghai Key Laboratory of Atmospheric Particle Pollution and Prevention, Department of Environmental Science and Engineering, Fudan University, Shanghai 200433, China

*Corresponding author: Dr. Jun Li

Tel: +86-20-85291508; Fax: +86-20-85290706; E-mail: junli@gig.ac.cn

Corresponding author: Dr. Gan Zhang

Tel: +86-20-85290805; Fax: +86-20-85290706; E-mail: zhanggan@gig.ac.cn

Key points:

- Both the MAE_{365} and fossil sources contribution of WSOC were higher in Northern China.
- The fossil sources derived WSOC only exhibited higher light absorption capacity in cold seasons.
- The non-fossil sources derived WSOC exhibited significant seasonal variation, which was likely associated with corn residues burning.

Abstract

Water soluble organic carbon (WSOC) makes up a large fraction of organic carbon, which attracted great attention due to its light absorption properties and human health effects. Sources and light absorption properties of WSOC in 10 cities across China were studied by dual carbon isotope analysis and UV−visible spectrophotometer, respectively. Despite the dominate contribution of non-fossil sources, the fossil sources contribution of WSOC in China was higher than other regions across the world. The average MAE_{365} and fossil sources contribution of WSOC was 1.13 ± 0.37 m^2/gC and 39.9 ± 9.4%, both of which were higher in Northern China. The non-fossil sources contribution of WSOC and $MAE_{365, WSOC}$ exhibited significant seasonal variations with highest values during cold seasons, which was likely associated with corn residues burning. Compared to warm seasons, the $MAE_{365, WSOC}$ showed a positive relationship with relative contribution of fossil sources and with higher values during cold seasons, indicating the fossil derived WSOC had higher light absorption capacity and enhance the overall color of WSOC during cold seasons. To constraining the regional climate and health impact of WSOC, this study suggests that mitigation strategy should consider the spatiotemporal variations in the sources, formation pathways and light absorption properties of WSOC.

Keywords: Water soluble organic carbon, Dual carbon isotope, Light absorption properties, China

1. Introduction

Water soluble organic carbon (WSOC) contributes approximately 20 to 90% of the OC, which could enhance the cloud condensation nuclei activity of particle and thus exert an indirect aerosol climate effects [*Kirillova et al.*, 2014b; *Zhang et al.*, 2018]. However, there is growing evidence that a certain fraction of WSOC could also absorb solar radiation directly and efficiently, particularly at shorter wavelength (< 400nm), which is contributor to brown carbon (BrC)[*Andreae and Gelencser*, 2006; *Laskin et al.*, 2015]. Recent studies showed that the dominant carbonaceous light−absorbing species is element carbon (EC), while the solar absorption of WSOC could be comparable to that of EC at ultraviolet wavelengths. [*Kirillova et al.*, 2016; *Srinivas et al.*, 2016; *Srinivas and Sarin*, 2014]. Therefore, the WSOC contributions of light absorbing at lower wavelength cannot be ignored, which could offset cooling effect of OC, influence tropospheric photochemistry and decrease ozone formation rates, especially in the biomass burning dominated regions (e.g., South and East Asia, South America, and subtropical Africa)[*Bahadur et al.*, 2012; *Chung et al.*, 2012; *Feng et al.*, 2013; *Ramanathan and Carmichael*, 2008]. In addition, WSOC may affect human health by catalyzing the generation of reactive oxygen species [*Lin and Yu*, 2011; *Verma et al.*, 2012].

The light absorption properties of WSOC could be highly source dependent [*Chung et al.*, 2012; *Desyaterik et al.*, 2013; *Feng et al.*, 2013; *Lambe et al.*, 2013]. However, the source apportionment of WSOC is still a challenge, due to its complex formation processes and a wide range of primary and secondary sources. Compared to methods associated with organic tracers and diagnostic mass ratios, dual carbon isotopes are intrinsic property of the carbonaceous aerosol, which can be used as more reliable tools for precise source apportionment of carbonaceous aerosol [*Bikkina et al.*, 2016; *Yan et al.*, 2018]. Radiocarbon (^{14}C) analysis is a powerful tool to quantitatively constrain relative contribution of fossil (e.g., coal and liquid fossil fuel) and non-fossil (e.g., biogenic emissions and biomass burning) sources of carbonaceous aerosol with high precision [*Szidat*, 2009; *Szidat et al.*, 2004], but the sources information

78 provided by ^{14}C is limited. In addition, stable carbon isotopes (^{13}C) can provide more information on
79 sources and atmospheric processes of carbonaceous aerosol.[*Bikkina et al.*, 2016; *Bosch et al.*, 2014b;
80 *Kirillova et al.*, 2014b]. Therefore, the combination of the isotopic signatures of ^{13}C and ^{14}C would
81 facilitate the determination of sources and atmospheric processes of WSOC.

82 China as a country with high loadings of anthropogenic carbonaceous aerosols, to accurately
83 understand the spatiotemporal variation of sources and light absorption properties of WSOC in China is
84 important for constraining the uncertainties of WSOC climate effects. Therefore, the objectives of this
85 study were (1) to investigate spatiotemporal variations of concentrations and light absorption properties of
86 WSOC across ten representative urban cities in China; (2) to determine sources of WSOCby \dual-carbon
87 isotope analysis; (3) to study the relationship between the light absorption properties and sources of
88 WSOC.

89

90 **2. Material and Methods**

91 **2.1 Sample collection and preparation.**

92 $PM_{2.5}$ samples were collected in 10 Chinese cities across four seasons (Table S1), including 4 in
93 Northern China (Beijing(BJ), Xinxiang(XX), Lanzhou(LZ), Taiyuan(TY)) and 6 in Southern China
94 (Shanghai(SH), Nanjing(NJ), Chengdu(CD), Guiyang(GY), Wuhan(WH), Guangzhou(GZ)). We divide
95 the cities according to annual average temperature and geographical location. The average annual
96 temperature of Northern cities is usually below 15 °C, while that of Southern cities is usually higher than
97 15 °C. At each site, aerosol samples were collected for 24h on pre-combusted (450 °C for 5 h) Whatman
98 quartz microfiber filters (8 × 10 in) using high-volume sampler operated at ~1000L/min. Four sampling
99 campaigns were conducted, 22 October 2013 to 13 November 2013, 30 December 2013 to 20 January
100 2014, 30 March to 20 April 2014, and 26 June to 24 August 2014, to represent fall, winter, spring and
101 summer, respectively. 995 samples were collected during the sampling periods. During each season, a
102 circle with 20 mm diameter was cut from each piece of filter and then pooled into a single sample (except

GY, where only fall and winter samples were collected). On average, ~ 26 samples were combined into a pooled sample. In total, 38 pooled samples were used in the subsequent experiments. For each site, one pooled sample was obtained for each season, and correspondingly, the analytical results represented seasonal averages. The urban rates of the provinces where the sampling sites are located ranged from 37.8 to 88.0% (National Bureau of Statistics, 2013, Table S1) [*China*, 2013], so the sampling sites can represent the regions of different developing levels in China. Based on the Chinese average urbanization rate in 2013 (54.8%), we classified the studied regions into the developing regions (< 60%) and developed regions (> 60%) in this work.

2.2 Extraction, water-soluble ions and light absorption measurements

The pooled sample was extracted with 100 mL ultrapure water (18.2 MΩ, Sartorius) under ultrasonication (30 min × 3 times), and then the water extracts were filtered through a 0.22-μm PTFE membrane (Jinteng, China) to remove insoluble particles.

The carbon content of WSOC was analyzed by a Total Organic Carbon analyzer (TOC-VCPH, Shimadzu). The relative standard deviation was 3.5%. 10 mL water extracts were used for water soluble ions analysis (Cl^-, NO_3^-, SO_4^{2-}, Na^+, K^+ and NH_4^+) by a Metrohm ion chromatograph (Model 761 compact IC). One replicated injection was carried out for every ten sample runs. The relative standard deviations were estimated to be less than 4%. All the amount of WSOC and water soluble ions presented in this study was corrected with field blank.

The absorption spectra of WSOC was recorded from 200 to 800 nm relative to ultrapure water by a UV-visible spectrophotometer (UV-4802, Unico, China). The mass absorption efficiency (MAE) was calculated according to previous studies [*Chen and Bond*, 2010; *Mo et al.*, 2017].

$$MAE_{\lambda} = \frac{|¿_{\lambda}|}{C_i} = \frac{\left(A_{\lambda} - A_{700}\right) \times \frac{V_{water}}{V_{air} \times l} \times \ln(10)}{C_i} ¿ \quad (1)$$

Where Abs_{λ} is the light absorption coefficient (Mm^{-1}); C_i is the corresponding concentration of

WSOC in the air (μgC/m^3); V_{water} is the volume of water; V_a is the volume of air sampled through the filter; l is the optical path length (in this study, 0.01 m); A_λ is light absorption of the solution at a given wavelength. The average light absorption between 695 and 705 nm (A_{700}) was used to account for baseline drift during analysis. The MAE_λ is presented at 365 nm (MAE_{365}, in m^2/gC) to compare with other studies and avoiding interferences from inorganic compounds (e.g., nitrate).

The wavelength dependence of different fraction absorption can be investigated by fitting the absorption Ångström exponent (AAE) by the following relation:

$$|¿_\lambda| = K \times \lambda^{-AAE} ¿ \quad (2)$$

The AAE is calculated by a linear regression of $\ln(Abs_\lambda)$ on $\ln(\lambda)$ within the range 330-400 nm for the avoidance of interference by inorganic species.

2.3 Stable carbon and radiocarbon analyses

The stable ($\delta^{13}C$) and radiocarbon ($\Delta^{14}C$) composition of WSOC were determined by Finnigan MAT-252 mass spectrometer (Thermo Electron Corporation, USA) and compact accelerator mass spectrometry instrument (NEC, National Electrostatics Corporation, USA) at the Guangzhou Institute of Geochemistry, respectively [*Zhu et al.*, 2015]. The details can be found in Supporting Information.

2.4 Bayesian mixing model

An advanced Bayesian mixing model was employed to quantify WSOC sources into liquid fossil fuel, coal combustion, C3 and C4 plants. The particular model framework and computing method could be found in previous study [*Zong et al.*, 2017]. In this model, the sources were firstly separated into fossil (liquid fossil fuel and coal combustion) and non-fossil sources (C3 and C4 plants) by the radiocarbon results, and then the contribution of each source was further confirmed by the stable carbon signatures. The sources end-members for $\delta^{13}C$ are summarized in Table S2. It should be noted that atmospheric processes (e.g., SOA formation and aging) may introduce uncertainties in the source apportionment results, because the source signatures ($\delta^{13}C$) of WSOC may be changed by the atmospheric processes.

However, WSOC as a complex mixture of highly polar compounds, it is difficult to quantify isotopic fractionation of WSOC during the complex atmospheric processes (e.g., SOA formation and aging). Therefore, the uncertainties of this model might be high, and the results of the calculation just as a supplementary evidence. In this work, the interquartile ranges (25^{th} to 75^{th}) of the model results were calculated to represent the uncertainties (Figure S2).

3. Results and Discussion

3.1 Spatiotemporal variation of concentration and light absorption of WSOC

The concentrations of WSOC ranged from 2.68 to 15.6 μgC/m^3 (6.88 ± 3.09 μgC/m^3, Table S3). As Figure 1a shows, the average concentrations of WSOC in Northern China were significantly higher than those in Southern China (8.28 ± 3.44 μgC/m^3 *v.s* 5.86 ± 2.41 μgC/m^3, $p < 0.01$). In addition, significant seasonal variations in the WSOC were observed. We found that WSOC exhibited lowest concentration during summer (3.99 ± 1.04 μgC/m^3), followed by spring (5.66 ± 2.08 μgC/m^3), fall (6.99 ± 1.99 μgC/m^3) and winter (10.4 ± 2.60 μgC/m^3). The lower WSOC concentrations during summer were likely associated high wet scavenging effects due to abundant precipitation, and favorable metrological conditions (e.g., higher boundary layer height, temperature and wind speed) for pollution dispersions (Table S4). Besides, the higher temperature in summer may decrease emissions from coal and biomass combustion for domestic/central heating, which might also lead to the lower WSOC concentrations. However, we found that the difference of WSOC between Northern China and Southern China was relatively small during summer (18.1% difference), but larger during other three seasons (71.2% difference in spring, 54.5% difference in fall and 38.0% difference in winter, Figure 1b). Given the fact that the temperature is relative higher in Southern China, the spatial variations in WSOC are most likely due to the increase in coal and biofuel combustion for domestic/central heating during the cold period in Northern China. Indeed, a previous study showed that more than 70% of annual OC emitted from coal and biofuel

combustion for residential heating in the North China Plain [*Liu et al.*, 2016b]. In addition, the lower spatial difference of WSOC concentration during summer also may be likely associated with the strong atmospheric convection and dispersion as explained above.

The light absorption at 365 nm (Abs_{365}) was widely used as BrC indicator. The averaged Abs_{365} values of WSOC ($Abs_{365,\ wsoc}$) were 8.57 ± 6.00 Mm^{-1} (1.60–25.7 Mm^{-1}, Figure 2). The $Abs_{365,\ wsoc}$ was correlated well with the concentrations of WSOC (r = 0.94, p < 0.01), so we observed the seasonal (winter > fall > spring > summer) and spatial (Northern China > Southern China) of Abs_{365} varied with the concentrations of WSOC. However, it is noteworthy that the light absorption of WSOC may be also affected by the sources of chromophores. For examples, biomass burning was reported as an important source of WSOC with high light absorption capacity [*Chen and Bond*, 2010; *Desyaterik et al.*, 2013; *Fan et al.*, 2016], and the biomass burning tracer K^+ had a higher correlation with $Abs_{365,\ wsoc}$ during cold seasons (r = 0.74, p < 0.01, Table S6). This indicated that in addition to the higher concentration of WSOC, the enhanced biomass burning emissions may be also one of important reasons for the higher $Abs_{365,\ WSOC}$. Contrary to the cold seasons, the relationship between $Abs_{365,\ WSOC}$ and K^+ were weaker (r = 0.54, p < 0.05), but the correlation between $Abs_{365,\ WSOC}$ and secondary inorganic ions were stronger during warm seasons (Table S6), indicating that the chromophores were more derived from secondary formations during warm seasons. This is consistent with previous studies reported that the secondary WSOC usually has a lower light absorption capacity, especially for those formed from biogenic precursors [*Lambe et al.*, 2013; *Li et al.*, 2016a]. Therefore, the seasonal difference in the sources of chromophores may also lead to the variation of $Abs_{365,\ wsoc}$. Finally, it should be noted that light absorption measured by solvent extracts may be different from those in ambient aerosols, considering the size distribution, effects of mixing state and morphology of particles [*Bahadur et al.*, 2012; *Chen et al.*, 2017]. To predict corresponding BrC absorption in ambient aerosols, the correction factors should be applied

[*Liu et al.*, 2013b].

The absorption Ångström Exponent (AAE) represents the wavelength dependence of the light absorption of BrC. The average AAE values of WSOC was 5.3 ± 0.6 (3.8–6.8, Table S5). The AAE values of WSOC were comparable to those measured in source region of South and East Asia [*Bosch et al.*, 2014b; *Cheng et al.*, 2016; *Du et al.*, 2014b; *Kim et al.*, 2016; *Kirillova et al.*, 2014b; *Srinivas et al.*, 2016], but much lower than that of the Indo-Gangetic Plain outflow measured over the Bay of Bengal during winter [*Srinivas et al.*, 2016]. It has been showed that AAE value could be highly dependent on the sources and atmospheric processes. Previous studies proposed that the AAE of WSOC from coal combustion (~4.4) was lower compared to biomass burning (~7–16) [*Chen and Bond*, 2010; *Shen et al.*, 2017]. Moreover, secondary organic aerosol (SOA) was shown to have higher AAE values compared with primary organic aerosol (POA) [*Saleh et al.*, 2013], but the AAE values might be decreased in the ammonium-mediated aging processes [*Bones et al.*, 2010]. However, the AAE values did not exhibit a clear seasonal and spatial variation ($p > 0.05$) in this study, indicating that the complexity of organic aerosol composition. Therefore, this work cannot clearly explain the relationship between AAE values and sources, on which further research work needs to be done.

The light absorption capacity of BrC was characterized by mass absorption efficiency at 365 nm (MAE_{365}). As shown in Table S5, the average MAE_{365} of WSOC ($MAE_{365,WSOC}$) was 1.13 ± 0.37 m^2/gC (0.55–1.86 m^2/gC), falling in the range of values observed at urban sites in South and East Asia (0.4–1.22 m^2/gC for Beijing, 1.54 ± 0.16 m^2/gC for Seoul, 1.3 ± 0.7 m^2/gC for Patiala and 1.6 ± 0.5 m^2/gC for New Delhi) [*Cheng et al.*, 2011; *Cheng et al.*, 2016; *Cheng et al.*, 2017; *Du et al.*, 2014a; *Kim et al.*, 2016; *Kirillova et al.*, 2014b; *Srinivas et al.*, 2016], but higher than those reported in Southeastern USA (0.21–0.77 m^2/gC) [*Bond et al.*, 2013; *Hecobian et al.*, 2010; *Zhang et al.*, 2011], East Asia and South Asia outflow sites (0.7 ± 0.2 m^2/gC for Jeju Island and 0.46 ± 0.18 m^2/gC for Hanimaadhoo Island) [*Bosch et al.*, 2014b; *Kirillova et al.*, 2014b], background sites over the northern Indian Ocean (0.45 ± 0.18 m^2/gC)

[*Srinivas and Sarin*, 2013], and high Himalayas (0.52 ± 0.18 m^2/gC) [*Kirillova et al.*, 2016]. The highest value of $MAE_{365, WSOC}$ was observed in TY (1.33 ± 0.43m^2/gC) in Northern China and lowest level occurred in GZ (0.84 ± 0.15m^2/gC) in Southern China. In general, the $MAE_{365, WSOC}$ values of WSOC exhibited significant spatial and seasonal variations. The $MAE_{365, WSOC}$ values during cold seasons were higher than those during warm seasons (1.38 ± 0.32 m^2/gC *v.s* 0.85 ± 0.17 m^2/gC, $p < 0.01$), and the $MAE_{365, WSOC}$ values in Northern China were higher than those in Southern China (1.25 ± 0.40 m^2/gC *v.s* 1.05 ± 0.33 m^2/gC, $p < 0.01$). Such variation of $MAE_{365, WSOC}$ might be attributed to the variability of sources, as discussed in section 3.3.

3.2 Dual carbon isotopes of WSOC

WSOC is an important component of carbonaceous aerosols that may derive from biomass burning and SOA formation. There is a need to better understand the sources of WSOC. Dual carbon isotopes analysis is a powerful tool to appoint the sources of carbonaceous aerosols, in which the radiocarbon isotope can directly distinguish between fossil and non-fossil sources and the stable carbon isotope can serve as a tracer to complement the information of sources and atmospheric processes [*Fang et al.*, 2017; *Kirillova et al.*, 2014a; *Kirillova et al.*, 2014b; *Yan et al.*, 2017]. The average non-fossil contribution to WSOC was 60.1 ± 9.4% (37.7–80.8%, Table S7), suggesting non-fossil sources were a dominant contributor of WSOC. The overwhelming non-fossil contribution to WSOC have been reported worldwide, but the non-fossil contribution of this work was lower than that of South Asia (71–92%) [*Bosch et al.*, 2014b; *Kirillova et al.*, 2013; *Kirillova et al.*, 2014b], U.S (67–100%) [*Weber et al.*, 2007; *Wozniak et al.*, 2012] and Europe (76–96%) [*Szidat et al.*, 2004; *Szidat et al.*, 2008], indicating that a larger influence of fossil sources to WSOC in China. It should be noted that only a small fraction of primary OC emitted from fossil sources was water soluble [*Fan et al.*, 2016; *Mo et al.*, 2017], thus, most of fossil derived WSOC might be secondary formed from fossil precursors. This was consistent with previous reports showed that a considerable fraction of secondary OC was fossil origin in China [*Xiang et*

246 *al.*, 2015; *Zhang et al.*, 2018].

247 Although the fossil sources contribution of WSOC in China was higher than those in other regions of
248 the world, it is lower than the fossil sources contribution of EC in China (> 70%) in previous reports
249 [*Andersson et al.*, 2015a; *Chen et al.*, 2013; *Zhang et al.*, 2015]. That might be due to relatively high
250 contribution to WSOC from primary and secondary formation from non-fossil emissions such as
251 biogenic, cooking and biomass-burning sources compared to EC. Indeed, compared with fossil fuel
252 combustion samples (coal combustion and diesel exhaust, WSOC/TC < 0.1), the WSOC/TC ratios were
253 significant lower for biomass burning emission sources (WSOC/TC > 0.3)[*Fan et al.*, 2016; *Li et al.*,
254 2018]. In addition, fossil components in water insoluble organic carbon (WISOC) were shown be
255 relatively more recalcitrant to further oxidative aging into WSOC than those of biomass burning/ biogenic
256 origins [*Bosch et al.*, 2014b; *Kirillova et al.*, 2014a; *Kirillova et al.*, 2013; *Kirillova et al.*, 2014b].
257 Moreover, chamber experiment found that the SOA formed from biogenic/biomass burning precursors
258 were all soluble in water, but those from fossil fuel precursors were less soluble in water but soluble in
259 methanol [*Updyke et al.*, 2012]. Therefore, the sources profile of WSOC should be more sensitive to
260 biomass/biogenic sources compared with EC.

261 As Figure 3 shows, the non-fossil contribution exhibited a clear seasonal variation with highest
262 values in fall (65.1 ± 7.1%, $p < 0.05$), followed by winter (61.9 ± 12.5%), spring (59.5 ± 7.1%) and
263 summer (53.2 ± 7.5%). Considering the biogenic volatile organic compounds (VOCs) emissions and
264 biogenic SOA was relative lower in China during cold seasons [*Ding et al.*, 2016a; *Ding et al.*, 2016b; *Li*
265 *et al.*, 2013], the higher non-fossil contribution during cold seasons was likely attributed to the
266 enhancement of biomass burning emissions during the harvest season or widespread usage of agricultural
267 waste for domestic heating. This was further confirmed by relative intensive active fire spots in cold
268 seasons (Figure S1). Meanwhile, the higher concentration of K^+ during cold seasons compared to warm
269 seasons (1.55 ± 0.65 μg/m^3 *v.s* 0.63 ± 0.29 μg/m^3, $p < 0.01$) and the higher correlation between the

concentration of K^+ and WSOC during cold seasons ($r = 0.79$, $p < 0.01$) than that during warm seasons ($r = 0.64$, $p < 0.01$, Tables S6). Previous studies also applied organic tracer, model and carbon isotope to show that biomass burning is an important source of OC during cold seasons in China [*Liu et al.*, 2017; *Liu et al.*, 2013a; *Liu et al.*, 2016b]. In addition, the stable carbon signature ($\delta^{13}C$) can provide more detail information for sources appointment, since the $\delta^{13}C$ of C4 plants (-19.3 to -12.3‰) and coal (-24.15 to -21.7‰) are higher than that of C3 plants (-34.7 to -24.6‰) and liquid fossil fuel (-29.0 to -23.6‰, summarized in Table S2). This study showed that $\delta^{13}C$ of WSOC in cold seasons were higher than those in warm seasons (-23.5 ± 0.7‰ v.s -24.7 ± 0.7‰, $p < 0.05$). Corn residue burning as the C4 plant could account for 15% of agricultural waste burning in China, which might be higher in fall [*Jin et al.*, 2018; *Li et al.*, 2016b]. A recent study also reported that more than 80% of the open straw burning released atmospheric pollutants is from corn residue burning in Northeast China [*Cui et al.*, 2020]. In addition, the Bayesian model results showed that the contribution of C4 plants to WSOC showed a significant seasonal variation pattern with highest values in fall (Figure S2), which is consistent with the fact that corn is usually planted in early summer and harvested in fall in China (Figure S3).The K^+ serve as a typical tracer for biomass burning, which also exhibit a better relationship with $WSOC_{C4\ plants}$ ($r = 0.84$, $p < 0.01$) than that of $WSOC_{C3\ plants}$ ($r = 0.65$, $p < 0.01$). Therefore, combined with ^{14}C results, the enrichment of ^{13}C during cold seasons could be mainly attributed to enhancement of C4 plants combustion (e.g., corn residues burning). In contrast, the lower non-fossil contribution and $\delta^{13}C$ values of WSOC during warm seasons, to some extent, could reflect the relative higher contribution of liquid fossil fuel.

In addition to sources, the $\delta^{13}C$ values could also reflect the atmospheric processes, since the $\delta^{13}C$ of OC may be changed by kinetic isotope effects (KIE) of atmospheric reactions. In the SOA formation processes, ^{13}C depletion occur as a result of organic compounds depleted in ^{13}C have a faster reaction rate[*Pavuluri and Kawamura*, 2016; *Zhou et al.*, 2017]. In contrast, in the photochemical aging processes, the high molecular compounds with lighter isotope react faster and release ^{12}C enriched short chain VOCs

or CO/CO_2, resulting in the remaining substrate enriched in ^{13}C due to KIE [*Kirillova et al.*, 2014a; *Kirillova et al.*, 2014b]. Therefore, the depletion of ^{13}C in WSOC during warm seasons might be attributed to the secondary formation of WSOC under stronger radiation and higher temperature, whereas the enrichment of ^{13}C in WSOC during cold seasons seemed to be related to aging processes. However, these possible causes are still speculative, our limited data cannot clearly distinguish the impact of two diametrically opposed effects on WSOC.

3.3 The influence of sources on light absorption capacity

Source plays an important role in light absorption capacity of BrC. Biomass burning is commonly regarded as the main emission source for BrC with high absorption capacity in field observations and model predictions [*Chung et al.*, 2012; *Desyaterik et al.*, 2013; *Feng et al.*, 2013]. Indeed, the $MAE_{365, WSOC}$ exhibited higher values with higher levels of K^+ and the non-fossil source contribution of WSOC during cold seasons in the nationwide (Figure 4a). Moreover, the correlation between $Abs_{365, WSOC}$ and K^+ during cool seasons ($r = 0.74$, $p < 0.01$) was stronger and more significant than that during warm seasons ($r = 0.54$, $p < 0.05$, Table S6). Thus, the higher $MAE_{365, WSOC}$ values during cold seasons may be related to the elevated biomass burning emissions. However, although the non-fossil contribution of WSOC in Northern China was lower than that in Southern China (55.6 ± 7.2% v.s 63.4 ± 9.5%, $p < 0.01$), the values of $MAE_{365, WSOC}$ in Northern China is still higher than that in Southern China (1.25 ± 0.40 m^2/gC *v.s* 1.05 ± 0.33 m^2/gC, $p < 0.01$, Figure 5b), indicating that besides biomass burning, the fossil derived WSOC may also have high light absorption capacity. Actually, it had been shown that the WSOC emitted from primary fossil fuel combustion exhibited a similar MAE_{365} value to that of biomass burning [*Du et al.*, 2014a; *Li et al.*, 2018; *Yan et al.*, 2017]. Furthermore, SOA formed from aromatic precursors emitted by fossil fuel combustion could also result in high MAE values [*Lambe et al.*, 2013; *Liu et al.*, 2016a]. Thus, the higher $MAE_{365, WSOC}$ in Northern China could be likely associated with higher fossil contribution. In

Northern Hemisphere (Figure 6), we found that the $MAE_{365, WSOC}$ values in East Asia (1.04 ± 0.40 m^2/gC) were comparable to those in South Asia (1.01 ± 0.45 m^2/gC), but significantly higher than those in USA and Europe (0.57 ± 0.43 m^2/gC, $p < 0.01$). To complement the ^{14}C-WSOC database by previous ^{14}C based source apportionment results summarized by *Zhang et al.* [2018], we found the fossil contribution of WSOC in East Asia (38.0 ± 11.6%, $p < 0.01$) is extremely higher than that in South Asia (18.0 ± 4.5%), USA and Europe (20.8 ± 7.6%). These indicate the higher light absorption capacity of WSOC in South Asia could be attributed to biomass burning emissions, while the higher absorption capacity of WSOC in East Asia were more associated with the fossil fuel combustion. Therefore, WSOC from both biomass burning and fossil sources has significant impacts on the OC radiative forcing.

To evaluate the relative importance of fossil and non-fossil sources to the WSOC light absorption, we investigate the relationship of fossil and non-fossil WSOC concentration with $Abs_{365, wsoc}$ by multiple linear regression model (Table S9). The unit of the unstandardized regression coefficients (m^2/gC) in the model could reflect the relative light absorption capacity of fossil and non-fossil WSOC to some extent. The regression coefficient of non-fossil WSOC (1.64 m^2/gC) was lower than that of fossil WSOC (2.15 m^2/gC), indicating the fossil derived WSOC exhibited higher light absorption capacity. This is consistent with the previous results showed that fossil sources were the important source of WSOC with high light absorption capacity [*Du et al.*, 2014b; *Lambe et al.*, 2013; *Li et al.*, 2018; *Liu et al.*, 2016a; *Yan et al.*, 2017]. Additionally, the lower unstandardized regression coefficients of non-fossil WSOC may be due to the fact that in addition to biomass burning with high light absorption capacity, the non-fossil sources also contain biogenic SOA with relatively low light absorption capacity. Furthermore, the relationship between the $MAE_{365, WSOC}$ and the relative contribution of fossil sources was studied (Figure 6). We found the relative contribution of fossil sources ($r = 0.52$, $p = 0.02$, Figure 6) showed a positive relationship with $MAE_{365, WSOC}$ in cold seasons, indicating the fossil sources derived WSOC in cold seasons had a higher light absorption capacity .That could be ascribed to coal combustion for heating in

Northern China might increase the emissions of WSOC with high light absorption capacity in winter [*Li et al.*, 2018; *Yan et al.*, 2017]. On the other hand, that may also be related to the SOA formation pathways. *Liu et al.* [2016a] showed that WSOC formed from fossil precursors (e.g., trimethylbenzene and toluene) under high-NO_x conditions have substantially higher light absorption capacity than those under low-NO_x condition. Given the fact that the concentration of NO_3^- was much higher in cold seasons compared to warm seasons (13.7 ± 6.4 μg/m^3 *v.s* 7.7 ± 5.1 μg/m^3, $p < 0.01$), the high light absorbing secondary fossil WSOC might be formed under relatively higher NO_x condition in cold seasons. While in the warm seasons, although there is no statistically significant, we found that the $MAE_{365, WSOC}$ decreased with the increasing contribution of fossil sources. As discussed above, the light absorption capacity of secondary fossil WSOC might be lower under the relatively lower NO_x formation condition, so those lower light absorbing secondary fossil WSOC might dilute the color of overall WSOC in warm seasons.

3.4 Implications

To implement effective strategy to mitigate the climate and health problems caused by WSOC, the sources of WSOC should be accurately identified and characterized. This work applied dual carbon isotopes to investigate the relationship between the sources and light absorption properties of WSOC. In addition, the seasonal and spatial scales data on sources and light absorption properties of WSOC over China in this work will help optimize the regional climate modeling and implement relevant regulation policy with respect to climate.

In this study, we found that both the biomass burning and fossil derived WSOC with high light absorption capacity, which is consistent with laboratory experiments and field observations [*Chung et al.*, 2012; *Desyaterik et al.*, 2013; *Feng et al.*, 2013; *Liu et al.*, 2016a]. We also observe that the fossil contribution of WSOC in the Chinese urban regions is higher than that in Europe and USA, which is likely due to large industrial and residential coal usage as well as vehicle emissions. Moreover, BC as the

dominant light-absorbing component of the aerosols, which is also mainly derived from fossil fuel combustion in China [*Andersson et al.*, 2015b; *Liu et al.*, 2017; *Liu et al.*, 2013a; *Zhang et al.*, 2018]. These implicate that mitigating emissions of carbonaceous particles from fossil fuel combustion could provide a good opportunity to reduce climate warming impact of both BC and light absorbing WSOC. However, it should be noted that, through correlation between fossil sources contribution and $MAE_{365, WSOC}$, we found that WSOC derived from fossil sources only exhibited higher light absorption capacity in cold seasons, which was likely associated with WSOC formation pathways [*Liu et al.*, 2016a]. Up until now, the few climate models have predicted the warming effects of BrC by assuming that absorption capacity of BrC is a constant value [*Feng et al.*, 2013; *Jo et al.*, 2016], which may introduce substantial uncertainties in predicting their climate impact. Therefore, to accurately assess the climate impact of BrC, the influence of different formation pathways on the light absorption properties of BrC should be considered in future climate models.

Despite the importance of contributions from fossil sources to WSOC, the non-fossil sources were still a major contributor of WSOC in Chinese urban regions, and the seasonal variation of $MAE_{365, WSOC}$ was associated with non-fossil sources. Especially, the non-fossil sources were shown to be highly related to human agricultural activities (e.g., corn residues burning) in this work. The crop residues burning could emit large amounts of nitrogen-containing organic compounds (NOC)[*Laskin et al.*, 2015]. Besides the nitroaromatic compounds that with high light absorption capacity, the nitrogen-containing bases (N-bases) are also major constituents of NOC [*Dou et al.*, 2015; *Lin et al.*, 2017; *Wang et al.*, 2017]. Moreover, the reversible redox sites in N-bases could catalyze the generation of reactive oxygen species which resulted in the adverse health effects [*Dou et al.*, 2015; *Wang et al.*, 2017]. Even in SH (with 88% urbanization rate), the contribution of non-fossil sources (66.4%) to WSOC was comparable to those in fall in developing regions (XX: 62.4%,CD: 72.2% WH:71.9% and GY: 74.6%, with urbanization < 60%), indicating the crop residues burning emissions in surrounding rural areas could also affect air quality and

people's health in densely populated urban areas. Therefore, the mitigation of emissions from agricultural residues burning during harvest season would be an effective mitigation strategy to counter climatic and health effects caused by WSOC.

The possible influence of WSOC on the climate and human health largely depend on its molecular compositions. Further experiments are needed to determine the molecular compositions of WSOC in order to link the sources of WSOC to their defining molecular characteristics, which in turn can be linked to environmental effects. In addition, the identification of the distinctive molecular from different emission sources (e.g., biogenic SOA, biomass burning, liquid fossil fuel and coal combustion) may help us find new organic tracers to accurately identify and quantify the sources of WSOC.

4. Conclusions

In present study, we investigated the sources and light absorption properties of WSOC in 10 cities across China. Despite a dominant non-fossil contribution to WSOC, the WSOC has higher fossil sources contribution (39.9 ± 9.4%) compared to other places in the world, suggesting a larger influence of fossil sources to WSOC in China. The fossil contribution and MAE_{365} of WSOC in Northern China (44.4 ± 7.3% and 1.25 ± 0.40 m^2/gC) were higher than those in Southern China (36.6 ± 9.5% and 1.05 ± 0.33 m^2/gC), which was probably related to larger fossil fuel consumption in Northern China. The non-fossil contribution and $MAE_{365, WSOC}$ exhibited a clear seasonal variation with highest values in fall (65.1 ± 7.1%), followed by winter (61.9 ± 12.5%), spring (59.5 ± 7.1%) and summer (53.2 ± 7.5%), which was likely associated with corn residues burning. The fossil sources derived WSOC exhibited higher light absorption capacity during cold seasons, which might be related to the WSOC formation pathways and coal combustion. Given the large spatiotemporal variation of sources, formation pathways and light absorption properties of WSOC, sources information provided by dual carbon isotope are crucial for making effective mitigation strategies to address the adverse effects of WSOC in China.

Acknowledgements

This study was supported by the Natural Science Foundation of China (NSFC; Nos. 41430645 and 41773120), the National Key R&D Program of China (2017YFC0212000) and Guangdong Foundation for Program of Science and Technology Research (Grant No. 2017B030314057). The original datasets for this research are available at Harvard Dataverse (https://dataverse.harvard.edu/privateurl.xhtml?token=17b8e313-f5ad-46a6-9240-41622ba7310d).We gratefully thank the people at all sites for sample collections and all of the individuals and groups participating in this project. This is a contribution of GIGCAS-2387.

References

Andersson, A., Deng, J., Du, K., Zheng, M., Yan, C., Sköld, M., Gustafsson, Ö. (2015a), Regionally-varying combustion sources of the January 2013 severe haze events over eastern China, *Environmental Science & Technology*, *49*(4), 2038-2043.

Andersson, A., Deng, J., Du, K., Zheng, M., Yan, C., Sköld, M., Gustafsson, O.r. (2015b), Regionally-varying combustion sources of the January 2013 severe haze events over eastern China, *Environmental Science & Technology*, *49*(4), 2038-2043.

Andreae, M.O., Gelencser, A. (2006), Black carbon or brown carbon? The nature of light-absorbing carbonaceous aerosols, *Atmospheric Chemistry and Physics*, *6*(10), 3131-3148.

Bahadur, R., Praveen, P.S., Xu, Y., Ramanathan, V. (2012), Solar absorption by elemental and brown carbon determined from spectral observations, *Proc Natl Acad Sci U S A*, *109*(43), 17366-17371, doi:10.1073/pnas.1205910109.

Bikkina, S., Andersson, A., Sarin, M., Sheesley, R., Kirillova, E., Rengarajan, R., Sudheer, A., Ram, K., Gustafsson, Ö. (2016), Dual carbon isotope characterization of total organic carbon in wintertime carbonaceous aerosols from northern India, *Journal of Geophysical Research: Atmospheres*, *121*(9), 4797-4809.

Bond, T.C., Doherty, S.J., Fahey, D.W., Forster, P.M., Berntsen, T., DeAngelo, B.J., Flanner, M.G., Ghan, S., Kaercher, B., Koch, D., Kinne, S., Kondo, Y., Quinn, P.K., Sarofim, M.C., Schultz, M.G., Schulz, M., Venkataraman, C., Zhang, H., Zhang, S., Bellouin, N., Guttikunda, S.K., Hopke, P.K., Jacobson, M.Z., Kaiser, J.W., Klimont, Z., Lohmann, U., Schwarz, J.P., Shindell, D., Storelvmo, T., Warren, S.G., Zender, C.S. (2013), Bounding the role of black carbon in the climate system: A scientific assessment, *Journal of Geophysical Research-Atmospheres*, *118*(11), 5380-5552, doi:10.1002/jgrd.50171.

Bones, D.L., Henricksen, D.K., Mang, S.A., Gonsior, M., Bateman, A.P., Nguyen, T.B., Cooper, W.J., Nizkorodov, S.A. (2010), Appearance of strong absorbers and fluorophores in limonene-O3 secondary organic aerosol due to NH4+-mediated chemical aging over long time scales, *Journal of Geophysical Research Atmospheres*, *115*(D5), D05203.

Bosch, C., Andersson, A., Kirillova, E.N., Budhavant, K., Tiwari, S., Praveen, P., Russell, L.M., Beres, N.D., Ramanathan, V., Gustafsson, Ö. (2014a), Source-diagnostic dual-isotope composition and optical properties of water-soluble organic carbon and elemental carbon in the South Asian outflow intercepted over the Indian Ocean, *Journal of Geophysical Research: Atmospheres*, *119*(20).

Bosch, C., Andersson, A., Kirillova, E.N., Budhavant, K., Tiwari, S., Praveen, P., Russell, L.M., Beres, N.D., Ramanathan, V., Gustafsson, Ö. (2014b), Source-diagnostic dual-isotope composition and optical properties of

water-soluble organic carbon and elemental carbon in the South Asian outflow intercepted over the Indian Ocean, *Journal of Geophysical Research: Atmospheres*, *119*(20), 11,743-711,759.
Chen, B., Andersson, A., Lee, M., Kirillova, E.N., Xiao, Q., Krusa°, M., Shi, M., Hu, K., Lu, Z., Streets, D.G. (2013), Source forensics of black carbon aerosols from China, *Environmental Science & Technology*, *47*(16), 9102-9108.
Chen, Q., Ikemori, F., Nakamura, Y., Vodicka, P., Kawamura, K., Mochida, M. (2017), Structural and light-absorption characteristics of complex water-insoluble organic mixtures in urban submicron aerosols, *Environmental Science & Technology*, *51*(15), 8293-8303.
Chen, Y., Bond, T.C. (2010), Light absorption by organic carbon from wood combustion, *Atmospheric Chemistry and Physics*, *10*(4), 1773-1787.
Cheng, Y., He, K.-B., Zheng, M., Duan, F.-K., Du, Z.-Y., Ma, Y.-L., Tan, J.-H., Yang, F.-M., Liu, J.-M., Zhang, X.-L. (2011), Mass absorption efficiency of elemental carbon and water-soluble organic carbon in Beijing, China, *Atmospheric Chemistry And Physics*, *11*(22), 11497-11510.
Cheng, Y., He, K.B., Du, Z.Y., Engling, G., Liu, J.M., Ma, Y.L., Zheng, M., Weber, R.J. (2016), The characteristics of brown carbon aerosol during winter in Beijing, *Atmospheric Environment*, *127*, 355-364.
Cheng, Y., He, K.B., Engling, G., Weber, R., Liu, J.M., Du, Z.Y., Dong, S.P. (2017), Brown and black carbon in Beijing aerosol: Implications for the effects of brown coating on light absorption by black carbon, *Science of the Total Environment*, *s 599–600*, 1047-1055.
China, N.B.o.S.o. (2013), *China statistical yearbook 2013*, ed., pp., Beijing.
Chung, C.E., Ramanathan, V., Decremer, D. (2012), Observationally constrained estimates of carbonaceous aerosol radiative forcing, *Proceedings of the National Academy of Sciences*, *109*(29), 11624-11629.
Cui, S., Song, Z., Zhang, L., Shen, Z., Hough, R., Zhang, Z., An, L., Fu, Q., Zhao, Y., Jia, Z. (2020), Spatial and temporal variations of open straw burning based on fire spots in northeast China from 2013 to 2017, *Atmospheric Environment*, 117962.
Desyaterik, Y., Sun, Y., Shen, X., Lee, T., Wang, X., Wang, T., Collett, J.L. (2013), Speciation of “brown” carbon in cloud water impacted by agricultural biomass burning in eastern China, *Journal of Geophysical Research: Atmospheres*, *118*(13), 7389-7399.
Ding, X., He, Q.F., Shen, R.Q., Yu, Q.Q., Zhang, Y.Q., Xin, J.Y., Wen, T.X., Wang, X.M. (2016a), Spatial and seasonal variations of isoprene secondary organic aerosol in China: Significant impact of biomass burning during winter, *Scientific reports*, *6*, 20411.
Ding, X., Zhang, Y.Q., He, Q.F., Yu, Q.Q., Shen, R.Q., Zhang, Y., Zhang, Z., Lyu, S.J., Hu, Q.H., Wang, Y.S. (2016b), Spatial and seasonal variations of secondary organic aerosol from terpenoids over China, *Journal of Geophysical Research Atmospheres*, *121*(24), 14,661-614,678.
Dou, J., Lin, P., Kuang, B.-Y., Yu, J.Z. (2015), Reactive oxygen species production mediated by humic-like substances in atmospheric aerosols: enhancement effects by pyridine, imidazole, and their derivatives, *Environmental Science & Technology*, *49*(11), 6457-6465.
Du, Z., He, K., Cheng, Y., Duan, F., Ma, Y., Liu, J., Zhang, X., Zheng, M., Weber, R. (2014a), A yearlong study of water-soluble organic carbon in Beijing I: Sources and its primary vs. secondary nature, *Atmospheric Environment*, *92*, 514-521.
Du, Z., He, K., Cheng, Y., Duan, F., Ma, Y., Liu, J., Zhang, X., Zheng, M., Weber, R. (2014b), A yearlong study of water-soluble organic carbon in Beijing II: Light absorption properties, *Atmospheric Environment*, *89*(2), 235-241.
Fan, X., Wei, S., Zhu, M., Song, J., Peng, P.A. (2016), Comprehensive characterization of humic-like substances in smoke PM2.5 emitted from the combustion of biomass materials and fossil fuels, *Atmospheric Chemistry & Physics*, *16*(20), 13321-13340.
Fang, W., Andersson, A., Zheng, M., Lee, M., Holmstrand, H., Kim, S.-W., Du, K., Gustafsson, Ö. (2017), Divergent evolution of carbonaceous aerosols during dispersal of East Asian haze, *Scientific reports*, *7*(1), 1-11.
Feng, Y., Ramanathan, V., Kotamarthi, V.R. (2013), Brown carbon: a significant atmospheric absorber of solar radiation?, *Atmospheric Chemistry & Physics*, *13*(17), 8607-8621.
Hecobian, A., Zhang, X., Zheng, M., Frank, N., Edgerton, E.S., Weber, R.J. (2010), Water-Soluble Organic Aerosol

material and the light-absorption characteristics of aqueous extracts measured over the Southeastern United States, *Atmospheric Chemistry And Physics*, *10*(13), 5965-5977.
Jin, Q., Ma, X., Wang, G., Yang, X., Guo, F.J.J.o.E.S. (2018), Dynamics of major air pollutants from crop residue burning in mainland China, 2000–2014, *Journal of Environmental Sciences*, *70*, 190-205.
Jo, D.S., Park, R.J., Lee, S., Kim, S.W., Zhang, X. (2016), A global simulation of brown carbon: implications for photochemistry and direct radiative effect, *Atmospheric Chemistry & Physics*, *15*(19), 27805-27852.
Kim, H., Jin, Y.K., Jin, H.C., Ji, Y.L., Lee, S.P. (2016), Seasonal variations in the light-absorbing properties of water-soluble and insoluble organic aerosols in Seoul, Korea, *Atmospheric Environment*, *129*(4), 234-242.
Kirillova, E.N., Andersson, A., Han, J., Lee, M., Gustafsson, Ö. (2014a), Sources and light absorption of water-soluble organic carbon aerosols in the outflow from northern China, *Atmospheric Chemistry and Physics*, *14*(3), 1413-1422.
Kirillova, E.N., Andersson, A., Sheesley, R.J., Kruså, M., Praveen, P., Budhavant, K., Safai, P., Rao, P., Gustafsson, Ö. (2013), 13C-and 14C-based study of sources and atmospheric processing of water-soluble organic carbon (WSOC) in South Asian aerosols, *Journal of Geophysical Research: Atmospheres*, *118*(2), 614-626.
Kirillova, E.N., Andersson, A., Tiwari, S., Srivastava, A.K., Bisht, D.S., Gustafsson, Ö. (2014b), Water-soluble organic carbon aerosols during a full New Delhi winter: Isotope-based source apportionment and optical properties, *Journal of Geophysical Research: Atmospheres*, *119*(6), 3476-3485.
Kirillova, E.N., Marinoni, A., Bonasoni, P., Vuillermoz, E., Facchini, M.C., Fuzzi, S., Decesari, S. (2016), Light absorption properties of brown carbon in the high Himalayas, *Journal of Geophysical Research Atmospheres*, *121*, 9621-9639.
Lambe, A.T., Cappa, C.D., Massoli, P., Onasch, T.B., Forestieri, S.D., Martin, A.T., Cummings, M.J., Croasdale, D.R., Brune, W.H., Worsnop, D.R. (2013), Relationship between oxidation level and optical properties of secondary organic aerosol, *Environmental science & technology*, *47*(12), 6349-6357.
Laskin, A., Laskin, J., Nizkorodov, S.A. (2015), Chemistry of atmospheric brown carbon, *Chemical reviews*, *115*(10), 4335-4382.
Li, C., Yan, F., Kang, S., Chen, P., Hu, Z., Gao, S., Qu, B., Sillanpää, M. (2016a), Light absorption characteristics of carbonaceous aerosols in two remote stations of the southern fringe of the Tibetan Plateau, China, *Atmospheric Environment*, *143*, 79-85.
Li, J., Bo, Y., Xie, S.J.J.o.E.S. (2016b), Estimating emissions from crop residue open burning in China based on statistics and MODIS fire products, *Journal of Environmental Sciences*, *44*, 158-170.
Li, L.Y., Chen, Y., Xie, S.D. (2013), Spatio-temporal variation of biogenic volatile organic compounds emissions in China, *Environmental Pollution*, *182*(6), 157-168.
Li, M., Fan, X., Zhu, M., Zou, C., Song, J., Wei, S., Jia, W., Peng, P.a. (2018), Abundance and Light Absorption Properties of Brown Carbon Emitted from Residential Coal Combustion in China, *Environmental Science & Technology*, *53*(2), 595-603.
Lin, P., Bluvshtein, N., Rudich, Y., Nizkorodov, S.A., Laskin, J., Laskin, A. (2017), Molecular Chemistry of Atmospheric Brown Carbon Inferred from a Nationwide Biomass Burning Event, *Environmental Science & Technology*.
Lin, P., Yu, J.Z. (2011), Generation of reactive oxygen species mediated by humic-like substances in atmospheric aerosols, *Environmental Science & Technology*, *45*(24), 10362-10368.
Liu, D., Li, J., Cheng, Z., Zhong, G., Zhu, S., Ding, P., Shen, C., Zhang, G. (2017), Sources of non-fossil fuel emissions in carbonaceous aerosols during early winter in Chinese cities, *Atmospheric Chemistry & Physics*, *17*(18), 1-25.
Liu, D., Li, J., Zhang, Y., Xu, Y., Liu, X., Ding, P., Shen, C., Chen, Y., Tian, C., Zhang, G. (2013a), The use of levoglucosan and radiocarbon for source apportionment of PM(2.5) carbonaceous aerosols at a background site in East China, *Environmental Science & Technology*, *47*(18), 10454-10461.
Liu, J., Bergin, M., Guo, H., King, L., Kotra, N., Edgerton, E., Weber, R. (2013b), Size-resolved measurements of brown carbon in water and methanol extracts and estimates of their contribution to ambient fine-particle light

absorption, *Atmospheric Chemistry and Physics*, *13*(24), 12389-12404.
Liu, J., Lin, P., Laskin, A., Laskin, J., Kathmann, S.M., Wise, M., Caylor, R., Imholt, F., Selimovic, V., Shilling, J.E. (2016a), Optical Properties and Aging of Light Absorbing Secondary Organic Aerosol, *Atmospheric Chemistry & Physics*, 1-36.
Liu, J., Mauzerall, D.L., Chen, Q., Zhang, Q., Song, Y., Peng, W., Klimont, Z., Qiu, X., Zhang, S., Hu, M. (2016b), Air pollutant emissions from Chinese households: A major and underappreciated ambient pollution source, *Proceedings of the National Academy of Sciences of the United States of America*, *113*(28), 7756.
Mo, Y.Z., Li, J., Liu, J.W., Zhong, G.C., Cheng, Z.N., Tian, C.G., Chen, Y.J., Zhang, G. (2017), The influence of solvent and pH on determination of the light absorption properties of water-soluble brown carbon, *Atmospheric Environment*, *161*, 90-98, doi:10.1016/j.atmosenv.2017.04.037.
Pavuluri, C.M., Kawamura, K. (2016), Enrichment of 13C in diacids and related compounds during photochemical processing of aqueous aerosols: New proxy for organic aerosols aging, *Scientific reports*, *6*.
Ramanathan, V., Carmichael, G. (2008), Global and regional climate changes due to black carbon, *Nature geoscience*, *1*(4), 221-227.
Saleh, R., Hennigan, C., McMeeking, G., Chuang, W., Robinson, E., Coe, H., Donahue, N., Robinson, A. (2013), Absorptivity of brown carbon in fresh and photo-chemically aged biomass-burning emissions, *Atmospheric Chemistry and Physics*, *13*(15), 7683-7693.
Shen, Z.X., Zhang, Q., Cao, J.J., Zhang, L.M., Lei, Y.L., Huang, Y., Huang, R.J., Gao, J.J., Zhao, Z.Z., Zhu, C.S., Yin, X.L., Zheng, C.L., Xu, H.M., Liu, S.X. (2017), Optical properties and possible sources of brown carbon in PM2.5 over Xi'an, China, *Atmospheric Environment*, *150*, 322-330, doi:10.1016/j.atmosenv.2016.11.024.
Srinivas, B., Rastogi, N., Sarin, M., Singh, A., Singh, D. (2016), Mass absorption efficiency of light absorbing organic aerosols from source region of paddy-residue burning emissions in the Indo-Gangetic Plain, *Atmos. Environ.*, *125*, 360-370.
Srinivas, B., Sarin, M. (2013), Light absorbing organic aerosols (brown carbon) over the tropical Indian Ocean: impact of biomass burning emissions, *Environmental research letters*, *8*(4), 044042.
Srinivas, B., Sarin, M. (2014), Brown carbon in atmospheric outflow from the Indo-Gangetic Plain: Mass absorption efficiency and temporal variability, *Atmospheric Environment*, *89*, 835-843.
Szidat, S. (2009), Atmosphere. Sources of Asian haze, *Science*, *323*(5913), 470-471, doi:10.1126/science.1169407.
Szidat, S., Jenk, T.M., H-A, S., Fisseha, R., Baltensperger, U., Kalberer, M., Samburova, V., Wacker, L., Saurer, M. (2004), Source Apportionment of Aerosols by 14C Measurements in Different Carbonaceous Particle Fractions, *Radiocarbon*, *46*(1), 475-484.
Szidat, S., Ruff, M., Perron, N., Wacker, L., Synal, H.A., Hallquist, M., Shannigrahi, A.S., Yttri, K.E., Dye, C., Simpson, D. (2008), Fossil and non-fossil sources of organic carbon (OC) and elemental carbon (EC) in G teborg, Sweden, *Atmospheric Chemistry & Physics*, *8*(5), 16255-16289.
Teich, M., Pinxteren, D.V., Wang, M., Kecorius, S., Wang, Z., Müller, T., Mocnik, G., Herrmann, H. (2017), Contributions of nitrated aromatic compounds to the light absorption of water-soluble and particulate brown carbon in different atmospheric environments in Germany and China, *Atmospheric Chemistry & Physics*, *17*(3), 1-24.
Updyke, K.M., Nguyen, T.B., Nizkorodov, S.A. (2012), Formation of brown carbon via reactions of ammonia with secondary organic aerosols from biogenic and anthropogenic precursors, *Atmospheric Environment*, *63*, 22-31.
Verma, V., Rico-Martinez, R., Kotra, N., King, L., Liu, J., Snell, T.W., Weber, R.J. (2012), Contribution of water-soluble and insoluble components and their hydrophobic/hydrophilic subfractions to the reactive oxygen species-generating potential of fine ambient aerosols, *Environmental Science & Technology*, *46*(20), 11384-11392.
Wang, Y., Hu, M., Lin, P., Guo, Q., Wu, Z., Li, M., Zeng, L., Song, Y., Zeng, L., Wu, Y. (2017), Molecular characterization of nitrogen-containing organic compounds in humic-like substances emitted from straw residue burning, *Environmental Science & Technology*, *51*(11), 5951-5961.
Weber, R.J., Sullivan, A.P., Peltier, R.E., Russell, A., Yan, B., Zheng, M., De Gouw, J., Warneke, C., Brock, C., Holloway, J.S. (2007), A study of secondary organic aerosol formation in the anthropogenic-influenced

598 southeastern United States, *Journal of Geophysical Research Atmospheres*, *112*(D13), D13302.
599 Wozniak, A.S., Bauer, J.E., Dickhut, R.M., Xu, L., Mcnichol, A.P. (2012), Isotopic characterization of aerosol
600 organic carbon components over the eastern United States, *Journal of Geophysical Research Atmospheres*,
601 *117*(D15), D13303.
602 Xiang, D., He, Q.F., Shen, R.Q., Yu, Q.Q., Wang, X.M.J.J.o.G.R.A. (2015), Spatial distributions of secondary
603 organic aerosols from isoprene, monoterpenes, β-caryophyllene and aromatics over China during summer, *Journal*
604 *of Geophysical Research Atmospheres*, *119*(20), 11,877-811,891.
605 Yan, C., Zheng, M., Bosch, C., Andersson, A., Desyaterik, Y., Sullivan, A.P., Collett, J.L., Zhao, B., Wang, S., He,
606 K. (2017), Important fossil source contribution to brown carbon in Beijing during winter, *Sci Rep*, *7*, 43182.
607 Yan, C., Zheng, M., Sullivan, A.P., Shen, G., Chen, Y., Wang, S., Zhao, B., Cai, S., Desyaterik, Y., Li, X. (2018),
608 Residential coal combustion as a source of levoglucosan in China, *Environmental Science & Technology*, *52*(3),
609 1665-1674.
610 Zhang, X., Lin, Y.-H., Surratt, J.D., Weber, R.J. (2013), Sources, composition and absorption Ångstrom exponent of
611 light-absorbing organic components in aerosol extracts from the Los Angeles Basin, *Environmental Science &*
612 *Technology*, *47*(8), 3685-3693.
613 Zhang, X., Lin, Y.H., Surratt, J.D., Zotter, P., Prévôt, A.S., Weber, R.J. (2011), Light-absorbing soluble organic
614 aerosol in Los Angeles and Atlanta: A contrast in secondary organic aerosol, *Geophysical Research Letters*,
615 *38*(21), L21810.
616 Zhang, Y.L., Elhaddad, I., Huang, R.J., Ho, K.F., Cao, J.J., Han, Y., Zotter, P., Bozzetti, C., Daellenbach, K.R.,
617 Slowik, J.G. (2018), Large contribution of fossil fuel derived secondary organic carbon to water soluble organic
618 aerosols in winter haze in China, *Atmospheric Chemistry & Physics*, *18*(6), 1-32.
619 Zhang, Y.L., Schnellekreis, J., Abbaszade, G., Zimmermann, R., Zotter, P., Shen, R., Schäfer, K., Shao, L., Prévôt,
620 A.S.H., Szidat, S. (2015), Source Apportionment of Elemental Carbon in Beijing, China: Insights from Radiocarbon
621 and Organic Marker Measurements, *Environmental Science & Technology*, *49*(14), 8408.
622 Zhou, Y., Xing, X., Lang, J., Chen, D., Cheng, S., Wei, L., Wei, X., Liu, C. (2017), A comprehensive biomass
623 burning emission inventory with high spatial and temporal resolution in China, *Atmos. Chem. Phys*, *17*(4), 2839-
624 2864.
625 Zhu, S., Ding, P., Wang, N., Shen, C., Jia, G., Zhang, G. (2015), The compact AMS facility at Guangzhou Institute
626 of Geochemistry, Chinese Academy of Sciences, *Nuclear Instruments & Methods in Physics Research*, *361*, 72-75.
627 Zong, Z., Wang, X., Tian, C., Chen, Y., Fang, Y., Zhang, F., Li, C., Sun, J., Li, J., Zhang, G. (2017), First
628 Assessment of NO x Sources at a Regional Background Site in North China Using Isotopic Analysis Linked with
629 Modeling, *Environmental Science & Technology*, *51*(11), 5923-5931.
630

633
634

Figure 1. Spatial (a) and seasonal (b) variations of WSOC in $PM_{2.5}$ from 10 Chinese cities (Note the abbreviation of the cities' name; Northern China: BJ-Beijing, XX-Xinxiang, TY-Taiyuan, LZ-Lanzhou; Southern China: SH-Shanghai, NJ-Nanjing, CD-Chengdu, GY-Guiyang, WH-Wuhan, GZ-Guangzhou).

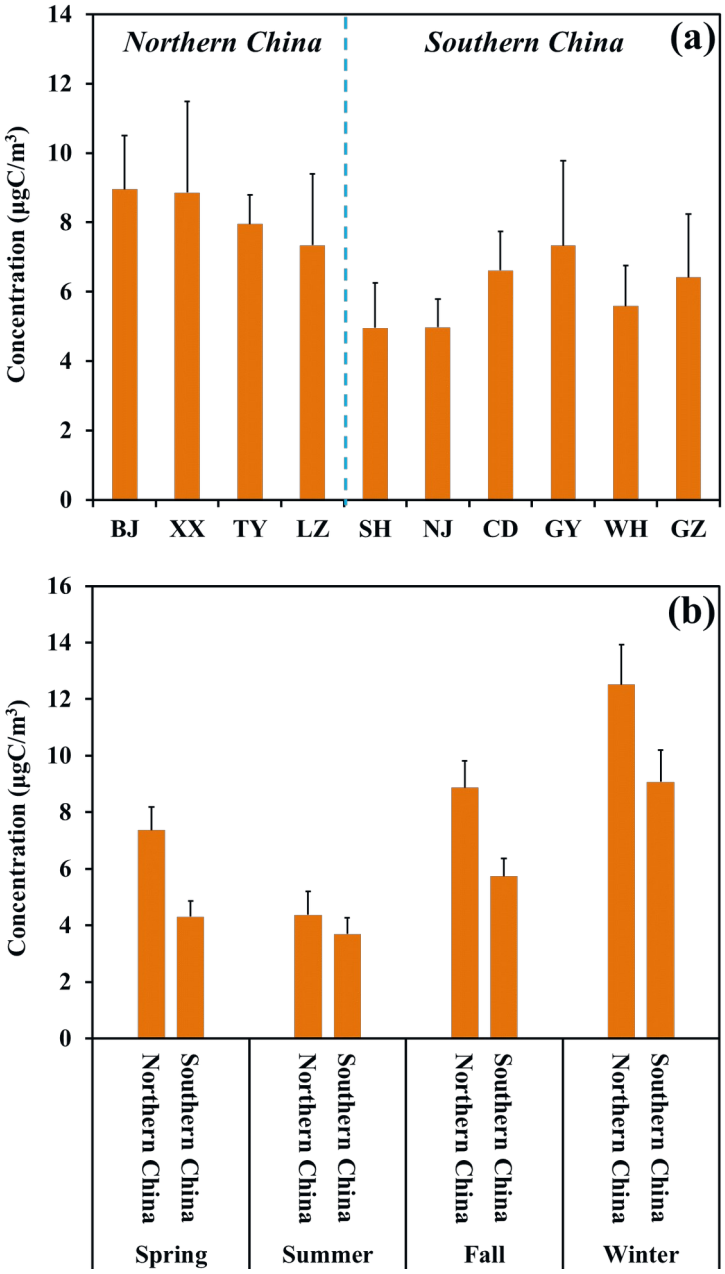

Figure 2. Spatial and seasonal variations of WSOC light absorption properties in $PM_{2.5}$ from 10 Chinese cities. The bars represent the light absorption coefficient at 365 nm (Abs_{365}, left axis), and the green lines represent the mass absorption efficiency at 365 nm (MAE_{365}, right axis).

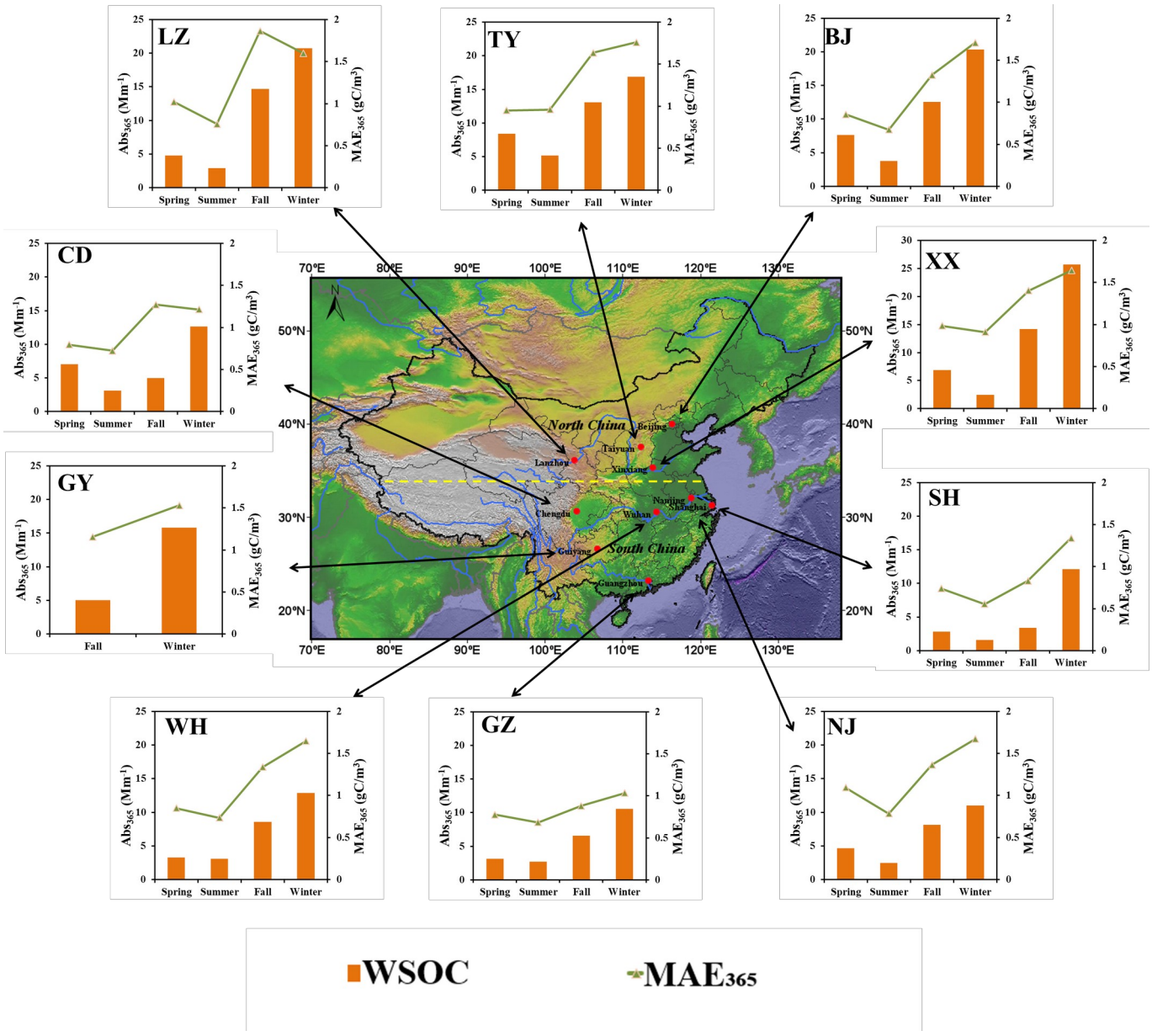

Figure 3. Dual carbon isotopes ($\Delta^{14}C$ versus $\delta^{13}C$) sources appointment of WSOC in different seasons (Spring: green, Summer: red, Fall: yellow and Winter: brown) over China. The expected $\delta^{13}C$ endmember ranges for C3 plants (light green, top), C4 plants (dark green, top), Liquid fossil fuel (black, bottom) and Coal (brown, bottom) are shown as rectangular bars (The $\delta^{13}C$ signature of sources endmember are summarized in Table S2).

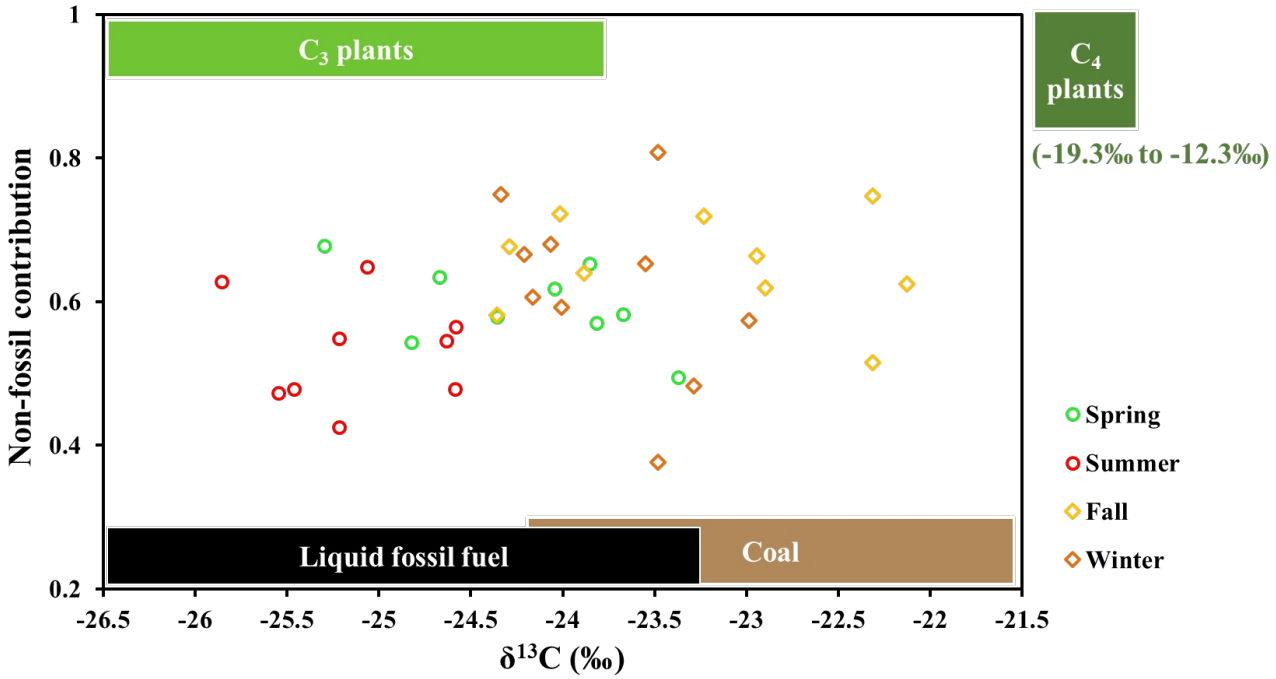

Figure 4. The (a) seasonal and (b) spatial variations of MAE_{365} and fossil sources contribution of WSOC over China.

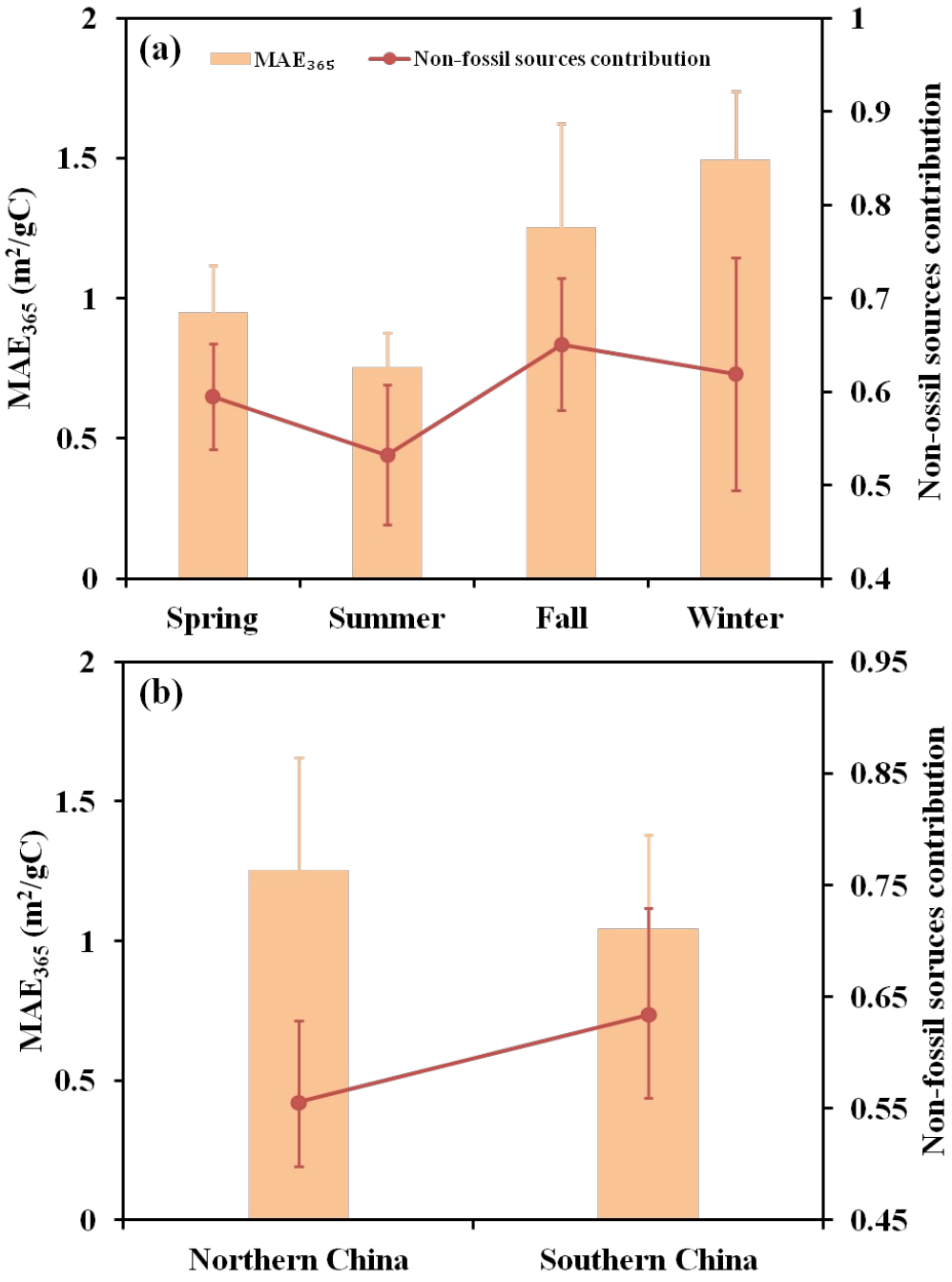

Figure 5. The MAE_{365} of WSOC in East Asia [*Cheng et al.*, 2011; *Cheng et al.*, 2016; *Cheng et al.*, 2017; *Du et al.*, 2014a; *Kirillova et al.*, 2014b; *Yan et al.*, 2017], South Asia [*Bosch et al.*, 2014a; *Kirillova et al.*, 2014b; *Srinivas et al.*, 2016; *Srinivas and Sarin*, 2013, 2014], the USA and Europe [*Hecobian et al.*, 2010; *Liu et al.*, 2013b; *Teich et al.*, 2017; *Zhang et al.*, 2013; *Zhang et al.*, 2011]. The box represents the 25th (lower line), 50th (middle line) and 75th (top line) percentiles; the empty square within the box represent the mean values; the end lines of the vertical bars represent the 10th (below the box) and 90th (above the box) percentiles; the x dots represent the maximum and minimum values; the solid diamonds represent the individual data.

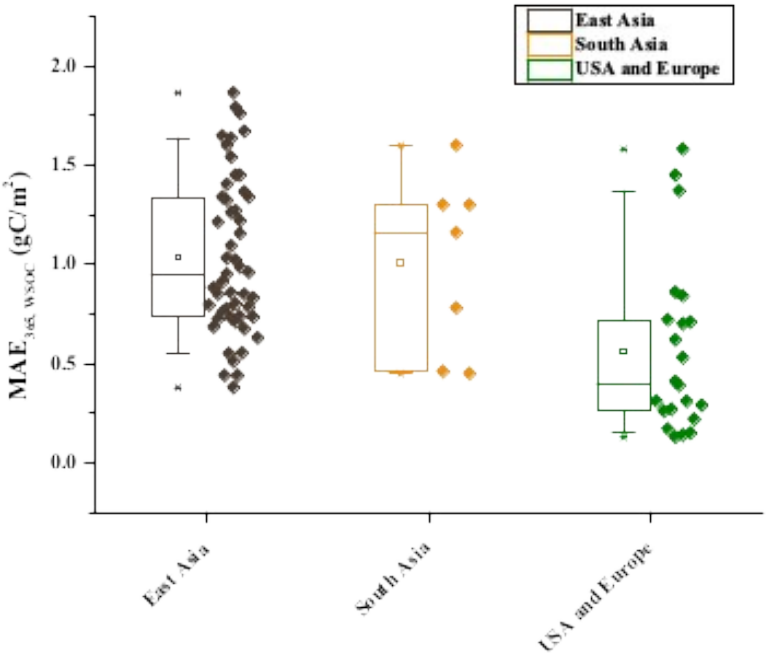

692 **Figure 6.** Correlation between $MAE_{365, WSOC}$ and relative contributions of fossil sources.

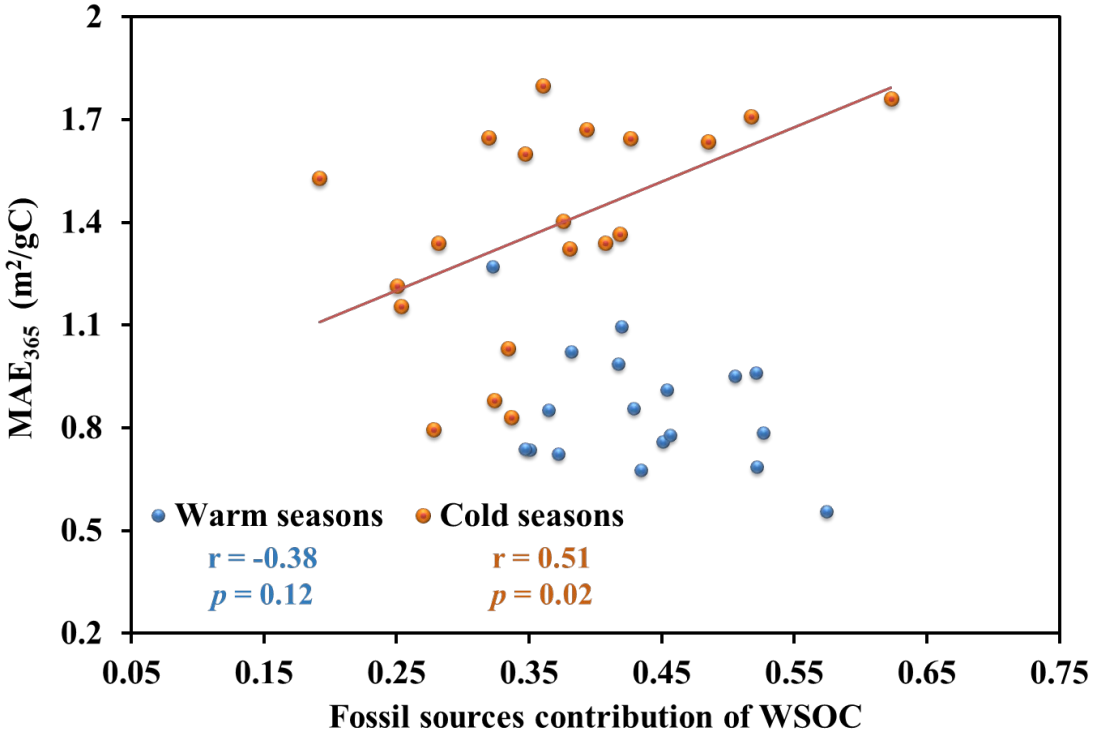

693

694

695

Supporting Information for

Dual carbon isotope-based source apportionment and light absorption properties of water soluble organic carbon in $PM_{2.5}$ over China

Yangzhi Mo[1], Jun Li[1*], Zhineng Cheng[1], Guangcai Zhong[1], Sanyuan Zhu[1], Chongguo Tian[2], Yingjun Chen[3], Gan Zhang[1*]

[1] State Key Laboratory of Organic Geochemistry and Guangdong Key Laboratory of Environmental Protection and Resources Utilization, Guangzhou Institute of Geochemistry, Chinese Academy of Sciences, Guangzhou 510640, China

[2] Key Laboratory of Coastal Zone Environmental Processes and Ecological Remediation, Yantai Institute of Coastal Zone Research, Chinese Academy of Science, Yantai, 264003, China

[3]Shanghai Key Laboratory of Atmospheric Particle Pollution and Prevention, Department of Environmental Science and Engineering, Fudan University, Shanghai 200433, China

*Corresponding author: Dr. Jun Li

Tel: +86-20-85291508; Fax: +86-20-85290706; E-mail: junli@gig.ac.cn

Corresponding author: Dr. Gan Zhang

Tel: +86-20-85290805; Fax: +86-20-85290706; E-mail: zhanggan@gig.ac.cn

Numbers of Pages: 15
Numbers of Tables: 9
Numbers of Figures: 3

Stable carbon and radiocarbon analyses

For stable carbon analysis, WSOC was extracted as described above. And then, 30–50 μgC of WSOC was re-dissolved in ultrapure water and transferred into a tin capsule (Elementar, Germany). After evaporation in an oven at 60°C, the stable isotopic composition ($\delta^{13}C$) was then measured using an elemental analyzer (EA, Model Vario Micro, Elementar, Germany) interfaced to a Finnigan MAT-252 mass spectrometer (Thermo Electron Corporation, USA). The $\delta^{13}C$ results were presented as relative to that of a standard, Vienna Pee Dee Belemnite. Samples were analyzed at least three times, and the analytical error in the carbon isotope ratios was within 0.3‰.

In a similar procedure to stable carbon analysis, more than 150 μg C of WSOC was packed in the tin capsules and then combusted to CO_2 by the elemental analyzer. Further, the CO_2 was reduced into graphite targets by graphitization line at Guangzhou Institute of Geochemistry of the Chinese Academy of Sciences (CAS) via the hydrogen and zinc reduction method and then the ^{14}C content of graphite samples was measured at the National Electrostatics Corporation compact accelerator mass spectrometry facility (AMS) at Guangzhou Institute of Geochemistry, CAS (Guangzhou, China)(Zhu et al., 2015). AMS calibration was performed using standards (Oxalic Acid Standards I and II) and blanks. The $\delta^{13}C$ value was obtained during AMS measurements and applied to correct the ^{14}C measurements for isotopic fractionation. The ^{14}C results are presented as fraction of modern (f_m) denoting the $^{14}C/^{12}C$ content of the sample related to that of the reference year 1950.(Levin et al., 2010; Mohn et al., 2008) To eliminate the effects of thermonuclear weapon tests in the 1950s and 1960s, the f_m was converted into the fraction of non-fossil carbon (f_{nf}) with a correction factor of 1.08 ± 0.05 based on the long-term time series of $^{14}CO_2$ at the background station, so the f_{nf} is calculated by $f_{nf} = f_m/1.08$. The f_{nf} can range from 0 (pure fossil carbon) to 1 (pure modern carbon) and directly reflects the relative fossil and non-fossil contribution to carbon. The uncertainties of f_{nf} was estimated from an error propagation, and included uncertainties in the concentration, variability of the reference $f_{m,nf}$, and measurement uncertainty of f_m. The average uncertainties of f_{nf} for WSOC was 2.79 ± 0.43 %.

Table S1. Information of sampling sites

Regions	Provrince (Urbanization rate %)[a]	City	Latitude (°N)	Longitude (°E)	Season	Samples Number
Northern China	Beijing (86.3)	Beijing (BJ)	39.93	116.34	Spring	29
					Summer	25
					Fall	22
					Winter	19
	Henan (39.3)	Xinxiang (XX)	35.33	113.91	Spring	29
					Summer	29
					Fall	21
					Winter	25
	Shanxi (52.6)	Taiyuan (TY)	37.54	112.33	Spring	31
					Summer	30
					Fall	26
					Winter	31
	Gansu (40.1)	Lanzhou (LZ)	36.05	103.86	Spring	28
					Summer	30
					Fall	27
					Winter	28
Southern China	Shanghai (88.0)	Shanghai (SH)	31.29	121.5	Spring	31
					Summer	23
					Fall	25
					Winter	29
	Jiangsu (62.9)	Nanjing (NJ)	32.06	118.8	Spring	22
					Summer	25
					Fall	25
					Winter	22
	Sichuan (44.9)	Chengdu (CD)	30.64	104.08	Spring	28
					Summer	29
					Fall	26
					Winter	30
	Guizhou (37.8)	Guiyang (GY)	26.57	106.73	Fall	22
					Winter	32
	Hubei (54.5)	Wuhan (WH)	30.53	114.37	Spring	23
					Summer	27
					Fall	22
					Winter	25
	Guangdong (67.8)	Guangzhou (GZ)	23.15	113.36	Spring	25
					Summer	27
					Fall	25
					Winter	22

[a] The urbanization rate of different provinces in 2013 was obtained from National Bureau of Statistics.

Table S2. The $\delta^{13}C$ values for source sampling reported in previous studies.

Sources	$\delta^{13}C$ values (‰)	$\delta^{13}C$ (‰) used in the Bayesian mixing model calculations (mean ± standard deviation).	References
Liquid fossil fuel	-29.0 to -23.6	-25.6 ± 1.8	(Agnihotri et al., 2011; Ancelet et al., 2011; Chen et al., 2012; Dai et al., 2015; Guo et al., 2016; Huang et al., 2006; Kawashima and Haneishi, 2012; López-Veneroni, 2009; Widory, 2006)
Coal combustion	-24.15 to -21.7	-23.4 ± 1.3	(Agnihotri et al., 2011; Chen et al., 2012; Guo et al., 2016; Kawashima and Haneishi, 2012; Widory, 2006)
C3 plants	-34.7 to -24.6	-28.2 ± 2.3	(Agnihotri et al., 2011; Ancelet et al., 2013; Chen et al., 2012; Das et al., 2010; Guo et al., 2016; Kawashima and Haneishi, 2012; Liu et al., 2014; Wang et al., 2013)
C4 plants	-19.3 to -12.3	-14.6 ± 2.6	(Chen et al., 2012; Das et al., 2010; Guo et al., 2016; Kawashima and Haneishi, 2012; Liu et al., 2014)

Table S3. Concentrations (ugC/m^3) of WSOC in $PM_{2.5}$ from 10 Chinese cities.

	Spring	Summer	Fall	Winter
Beijing	8.90	5.54	9.46	11.9
Xinxiang	7.00	2.68	10.1	15.6
Taiyuan	8.84	5.39	8.01	9.59
Lanzhou	4.70	3.85	7.87	12.95
Shanghai	3.82	2.89	4.06	9.05
Nanjing	4.25	3.13	5.95	6.57
Chengdu	5.53	4.30	6.23	10.4
Guiyang[a]	N.D	N.D	4.35	10.3
Wuhan	3.89	4.25	6.39	7.80
Guangzhou	4.02	3.92	7.46	10.3
AVG[a]	5.66	3.99	6.72	10.3
SD[b]	2.08	1.01	1.90	2.70

[a] Guiyang just contains fall and winter samples.
[b] AVG: Arithmetic average.
[c] SD: Standard deviation.

Table S4. The average temperature and precipitation at ten cities during the sampling campaign.

City	Temperature (℃)				Precipitation (mm)			
	Spring	Summer	Fall	Winter	Spring	Summer	Fall	Winter
BJ	17.0	26.3	10.3	0.3	20.8	52.3	12.6	3.0
XX	16.9	25.9	13.7	4.3	56.4	67.7	29.8	0.2
TY	14.5	23.0	10.6	0.5	55.6	131.1	37.6	18.8
LZ	21.7	28.5	19.3	0.1	135.0	244.6	60.4	84.9
SH	16.0	26.6	16.8	6.7	139.4	271.4	156.1	35.8
NJ	16.5	25.9	15.8	5.8	97.5	161.5	21.5	15.6
CD	20.3	28.2	17.7	9.3	93.6	239.9	74.0	11.1
GY	17.2	23.5	13.8	6.1	37.5	167.2	52.8	24.7
WH	17.7	26.7	15.8	6.1	107.3	145.5	30.1	19.5
GZ	23.2	29.0	22.0	13.7	192.7	513.3	23.6	53.0
AVG[a]	18.1	26.4	15.6	6.3	93.6	199.5	49.8	26.6
SD[b]	2.7	2.0	3.7	4.2	52.8	131.8	41.9	25.6

[a] AVG: Arithmetic average.
[b] SD: Standard deviation.

Table S5. MAE_{365} and AAE of WSOC in $PM_{2.5}$ from 10 Chinese cities.

	$MAE_{365}(m^2/gC)$				AAE			
	Spring	Summer	Fall	Winter	Spring	Summer	Fall	Winter
Beijing	0.86	0.67	1.32	1.71	5.7	5.2	6.8	5.6
Xinxiang	0.99	0.91	1.4	1.65	5.1	3.8	4. 8	5.2
Taiyuan	0.95	0.96	1.64	1.76	5.7	5.1	5.2	6.3
Lanzhou	1.02	0.76	1.86	1.6	5.7	5.2	4.2	4.7
Shanghai	0.74	0.55	0.83	1.34	5.4	5.7	5.6	5.3
Nanjing	1.09	0.78	1.37	1.67	4.9	5.3	4.9	5.1
Chengdu	0.79	0.72	1.27	1.21	5.3	5.7	5.7	5.7
Guiyang[a]	N.D	N.D	1.16	1.53	N.D	N.D	4.4	5
Wuhan	0.85	0.73	1.34	1.65	5.4	5.6	5.1	4.8
Guangzhou	0.78	0.68	0.88	1.03	6	5.9	5.8	5.8
AVG[b]	0.95	0.75	1.25	1.49	5.5	5.3	5.1	5.3
SD[c]	0.17	0.12	0.37	0.24	0.3	0.6	0.6	0.5

[a] Guiyang just contains fall and winter samples.
[b] AVG: Arithmetic average.
[c] SD: Standard deviation.

Table S6. Correlation coefficients (r) of Abs_{365} with WSOC and water soluble ions.

	$Abs_{365, WSOC}$	
	Warm seasons	Cold seasons
WSOC	0.92^{*}	0.92^{*}
K^+	$0.54^{\#}$	0.74^{*}
NO_3^-	0.85^{*}	$0.52^{\#}$
SO_4^{2-}	0.64^{*}	$0.56^{\#}$
NH_4^+	0.73^{*}	$0.48^{\#}$

* $p < 0.01$
$^{\#}$ $p < 0.05$

Table S7. The annual average $\delta^{13}C$ and non-fossil contribution of WSOC.

	$\delta^{13}C$ (‰)		Non-fossil contribution	
	WSOC	SD	WSOC	SD
Beijing	-23.7	0.7	0.56	0.06
Xinxiang	-23.4	1.1	0.58	0.03
Taiyuan	-23.4	0.9	0.47	0.06
Lanzhou	-24.2	0.7	0.61	0.05
Shanghai	-24	0.9	0.58	0.11
Nanjing	-24.6	0.6	0.56	0.06
Chengdu	-24.9	0.9	0.69	0.05
Guiyang[a]	-22.9	0.8	0.78	0.04
Wuhan	-24.3	0.8	0.67	0.04
Guangzhou	-24.7	0.6	0.59	0.1

[a] Guiyang just contains fall and winter samples.

Table S8. The annual average concentration of water soluble ions.

	Cl^-	SD	NO_3^-	SD	SO_4^{2-}	SD	K^+	SD	Na^+	SD	NH_4^+	SD
Beijing	2.58	2.17	14.0	5.89	11.6	1.96	1.05	0.51	0.59	0.32	7.84	2.49
Xinxiang	4.06	3.65	17.4	10.0	20.7	10.3	1.70	1.15	0.64	0.44	9.56	5.31
Taiyuan	6.43	6.06	14.5	5.96	27.2	4.21	1.49	0.70	0.96	0.54	9.87	1.96
Lanzhou	3.71	2.95	9.79	6.29	13.6	4.85	1.43	0.94	1.23	0.59	3.63	2.92
Shanghai	1.38	1.51	9.59	6.71	9.28	3.85	0.62	0.44	0.49	0.14	5.53	2.92
Nanjing	1.10	1.01	10.9	5.25	10.4	3.84	0.85	0.49	0.24	0.08	6.84	2.74
Chengdu	1.29	0.87	9.27	4.42	11.2	3.51	0.76	0.49	0.28	0.07	7.05	2.82
Guiyang[a]	0.41	0.29	4.22	3.71	15.5	5.97	0.90	0.44	0.17	0.09	6.32	2.65
Wuhan	0.74	0.80	8.86	5.23	11.7	2.55	0.92	0.45	0.20	0.04	6.52	2.13
Guangzhou	0.60	0.47	6.61	5.80	15.3	8.13	1.30	0.62	0.58	0.12	7.53	4.66

[a] Guiyang just contains fall and winter samples.

Table S9. Multiple linear regression between Abs_{365} and concentration of fossil and non-fossil sources WSOC in China.

Model: R^2 = 0.891 Adjusted R^2 = 0.884	Unstandardized coefficients		*t*-STAT	*p*-Value
	B	Standard error		
Constant	-4.127	0.801	-5.154	0.000
Fossil sources concentration	2.148	0.302	7.109	0.000
Non-fossil sources concentration	1.641	0.206	7.963	0.000

Figure S1. Cluster analysis of 5-day backward trajectories and the spatial distributions of active fire spots over China during the sampling campaign. Cluster analysis is performed by HYSPLIT. Red dots represent fire count data obtained from Fire Information for Resource Management System (FIRMS) acquired by the Moderate Resolution Imaging Spectroradiometer (MODIS) satellite for the sampling days. The basemap was created by ArcGIS software (Source: ESRI Inc. CA).

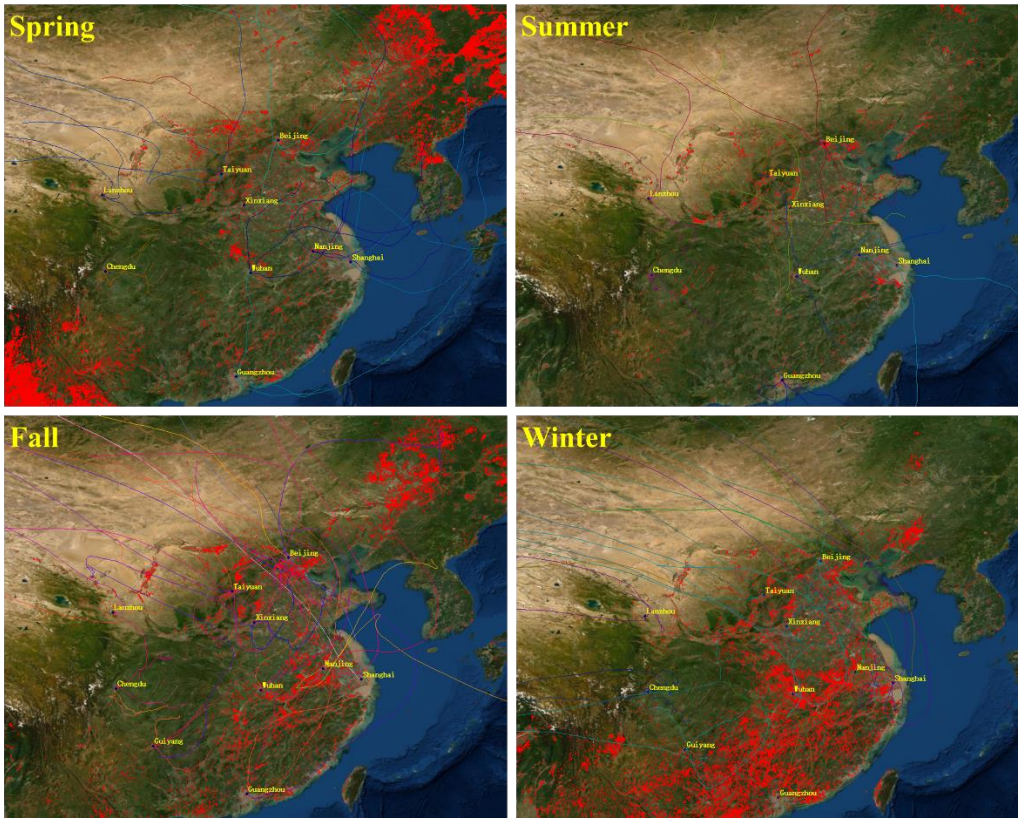

Figure S2. The median contributions and concentrations of liquid fossil fuel, coal combustion, C3 plants and C4 plants of WSOC by Bayesian source appointment model. The red line is the median of contribution and the orange region refers to the interquartile range (25^{th} to 75^{th}).

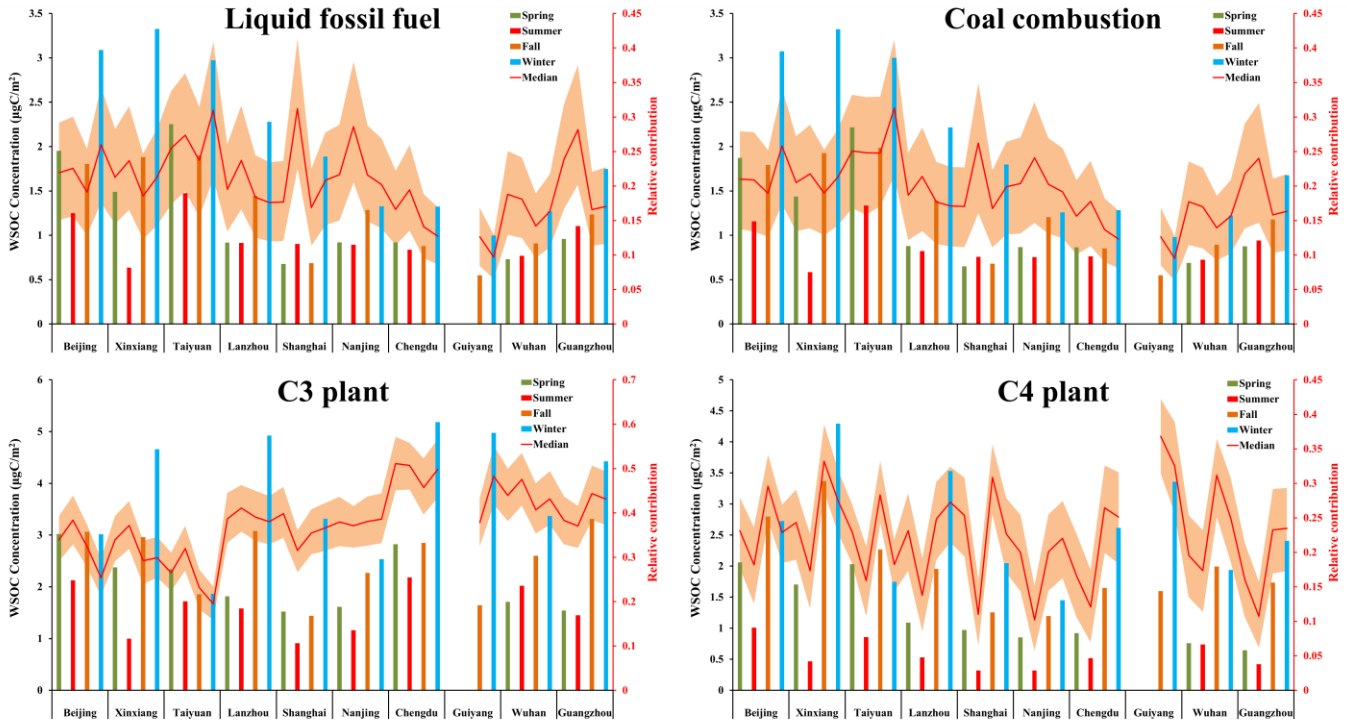

Figure S3. The distribution of main corn area in China. (https://www.fas.usda.gov/data/summer-drought-limits-upside-potential-china-corn-yields).

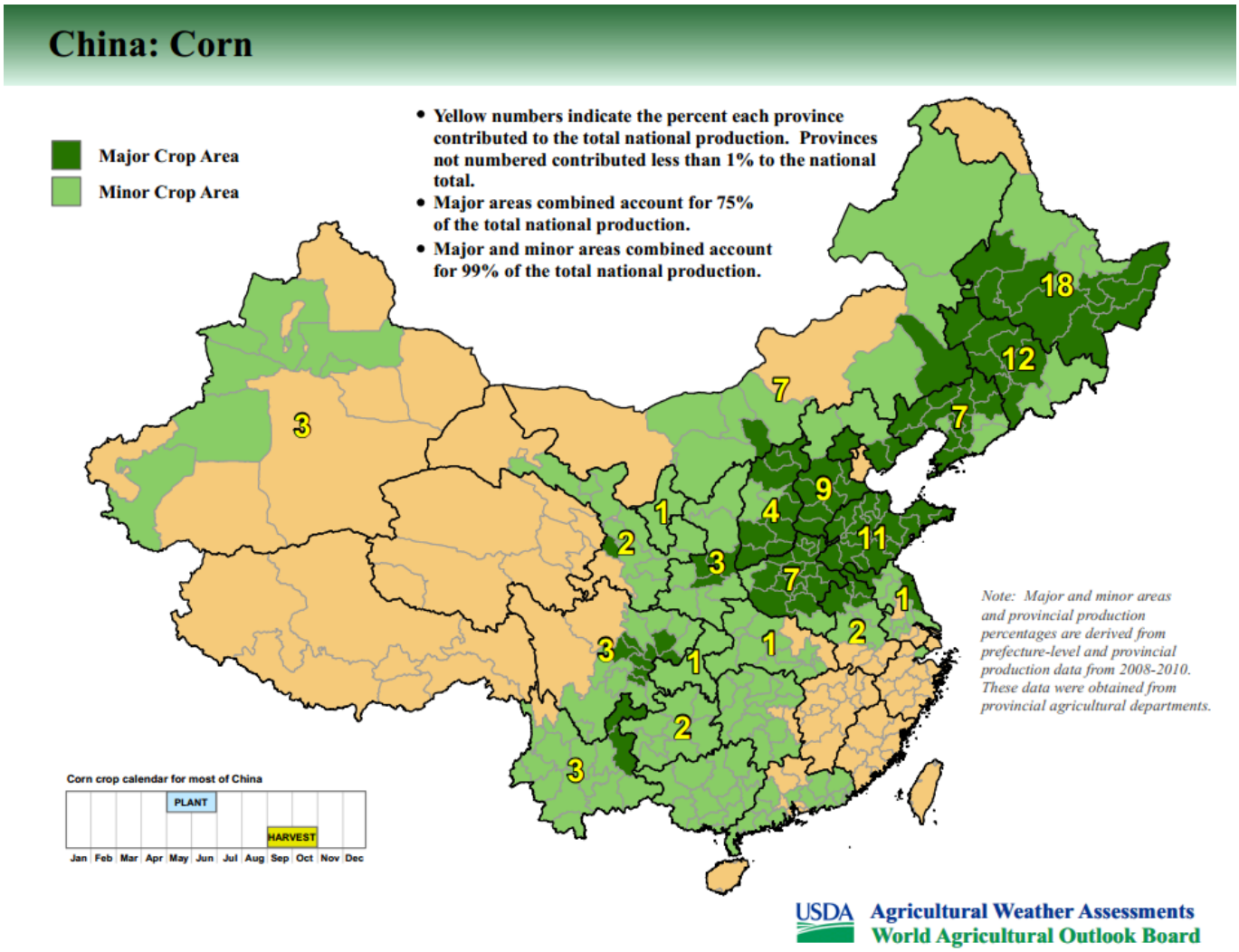

177
178

References:

Agnihotri, R., Mandal, T., Karapurkar, S., Naja, M., Gadi, R., Ahammmed, Y.N., Kumar, A., Saud, T., Saxena, M., 2011. Stable carbon and nitrogen isotopic composition of bulk aerosols over India and northern Indian Ocean. Atmospheric Environment 45, 2828-2835.

Ancelet, T., Davy, P.K., Trompetter, W.J., Markwitz, A., Weatherburn, D.C., 2011. Carbonaceous aerosols in an urban tunnel. Atmospheric Environment 45, 4463-4469.

Ancelet, T., Davy, P.K., Trompetter, W.J., Markwitz, A., Weatherburn, D.C., 2013. Carbonaceous aerosols in a wood burning community in rural New Zealand. Atmospheric Pollution Research 4, 245-249.

Chen, Y., Cai, W., Huang, G., Li, J., Zhang, G.J.H.j.k.x.H.k., 2012. Stable carbon isotope of black carbon from typical emission sources in China. 33, 673-678.

Dai, S., Bi, X., Chan, L., He, J., Wang, B., Wang, X., Peng, P., Sheng, G., Fu, J., 2015. Chemical and stable carbon isotopic composition of PM 2.5 from on-road vehicle emissions in the PRD region and implications for vehicle emission control policy. Atmospheric Chemistry and Physics 15, 3097-3108.

Das, O., Wang, Y., Hsieh, Y.-P.J.O.G., 2010. Chemical and carbon isotopic characteristics of ash and smoke derived from burning of C3 and C4 grasses. 41, 263-269.

Guo, Z., Jiang, W., Chen, S., Sun, D., Shi, L., Zeng, G., Rui, M.J.A.R., 2016. Stable isotopic compositions of elemental carbon in PM1. 1 in north suburb of Nanjing Region, China. 168, 105-111.

Huang, L., Brook, J., Zhang, W., Li, S., Graham, L., Ernst, D., Chivulescu, A., Lu, G., 2006. Stable isotope measurements of carbon fractions (OC/EC) in airborne particulate: A new dimension for source characterization and apportionment. Atmospheric Environment 40, 2690-2705.

Kawashima, H., Haneishi, Y., 2012. Effects of combustion emissions from the Eurasian continent in winter on seasonal δ 13 C of elemental carbon in aerosols in Japan. Atmospheric environment 46, 568-579.

Levin, I., Naegler, T., Kromer, B., Diehl, M., Francey, R.J., Gomez-Pelaez, A.J., Steele, L.P., Wagenbach, D., Weller, R., Worthy, D.E., 2010. Observations and modelling of the global distribution and long-term trend of atmospheric 14CO2. Tellus 62, 26-46.

Liu, G., Li, J., Xu, H., Wu, D., Liu, Y., Yang, H.J.A.e., 2014. Isotopic compositions of elemental carbon in smoke and ash derived from crop straw combustion. 92, 303-308.

López-Veneroni, D., 2009. The stable carbon isotope composition of PM 2.5 and PM 10 in Mexico City Metropolitan Area air. Atmospheric Environment 43, 4491-4502.

Mohn, J., Szidat, S., Fellner, J., Rechberger, H., Quartier, R., Buchmann, B., Emmenegger, L., 2008. Determination of biogenic and fossil CO2 emitted by waste incineration based on (CO2)-C-14 and mass balances. Bioresource Technology 99, 6471-6479.

Wang, G., Yao, J., Zeng, Y., Huang, Y., Qian, Y., Liu, W., Li, Y., Yuan, N., Liu, S., Shan, J., 2013. Source Apportionment of Carbonaceous Particulate Matter in a Shanghai Suburb Based on Carbon Isotope

214 Composition. Aerosol Science and Technology 47, 239-248.
215 Widory, D., 2006. Combustibles, fuels and their combustion products: A view through carbon isotopes.
216 Combustion Theory and Modelling 10, 831-841.
217 Zhu, S., Ding, P., Wang, N., Shen, C., Jia, G., Zhang, G., 2015. The compact AMS facility at Guangzhou
218 Institute of Geochemistry, Chinese Academy of Sciences. Nuclear Instruments & Methods in Physics
219 Research 361, 72-75.
220